SLAC–PUB–6634
October 1994
(A)

TRANSVERSE PROTON DIFFUSION*

F. ZIMMERMANN

Stanford Linear Accelerator Center
Stanford University, Stanford, CA 94309

A semi-analytical approach is described for evaluating diffusion rates due to different processes, such as Arnold diffusion, resonance streaming, modulational diffusion, and 'sweeping diffusion', in a proton storage ring. This approach makes use of parameters for high-order resonances in the transverse phase space, which may be obtained, for example, by normal-form algorithms using differential-algebra software, and is applied to the HERA proton ring at DESY. While neither Arnold diffusion nor resonance streaming nor sweeping diffusion can explain the dynamic aperture observed in HERA, the effect of modulational diffusion is consistent with the measurements.

KEY WORDS: Dynamic Aperture, Particle Dynamics, Superconducting Storage Rings

Submitted to Particle Accelerators

* Work supported by Department of Energy contract DE–AC03-76SF00515.

1 INTRODUCTION

Studies of the dynamic aperture and of transverse diffusion rates in proton storage rings are conventionally performed by means of extensive computer simulations. While these simulations require large amounts of computing power and time, their predictions suffer from inherent uncertainties arising from the limited (small) number of particles, turns and working points studied, from the question of applicability of the chosen stability criteria (for instance Lyapunov-exponent), and from the usual neglect of many, apparently insignificant, effects (for example tune drifts, decay of persistent-current field errors, ground motion, gas scattering, intra-beam scattering etc.), whose interplay with the nonlinear motion may prove important on a long time scale.

In this report we describe a semi-analytical approach to evaluate macroscopic (i.e., measurable) diffusion rates, which appears as a promising alternative to long-term tracking studies. The basic ingredients of this approach are

- a set of parameters of isolated, high-order resonances,
- local diffusion rates in the vicinity of a single resonance, and
- a method to combine the local diffusion rates at each resonance into a macroscopic 'global' diffusion rate, which may be compared with measurements.

The paper is structured as follows. Section 2 is devoted to a general description of the semi-analytical approach, in which the different diffusion mechanisms and a method of calculating the associated macroscopic diffusion rates are discussed. In Section 3 diffusion rates due to different processes are calculated for the HERA proton ring at DESY, using parameters of resonances through order 11, which are obtained by a normal-form analysis. It is shown that modulational diffusion may explain the difference between the measured dynamic aperture and that predicted by computer simulations. Results are summarized and some conclusions are drawn in Section 4. The appendices contain a review of single-resonance characteristics, re-derivations of local diffusion coefficients for modulational diffusion and Arnold diffusion, a brief description of simulation studies and aperture measurements in

HERA, and a discussion of the normal-form analysis along with a compilation of typical resonance parameters through order 11.

2 SEMI-ANALYTICAL CALCULATION OF DIFFUSION RATES

2.1 Diffusion Equation

Amplitude-dependent transverse diffusion rates determine the beam lifetime and are very important for background considerations as well as for the design of experiments in the beam halo. Observations[1,2,3] suggest that the transverse motion of stored protons is often well described by a diffusion equation of the form

$$\frac{\partial f}{\partial t} = \frac{\partial}{\partial I}\left(D(I)\frac{\partial f}{\partial I}\right) \tag{1}$$

where I denotes an appropriate action variable. Most proton storage rings are operated close to the linear coupling resonance $Q_x - Q_z = m$ (m integer), and in this case the action variable I may be chosen as the total transverse action $I \equiv I_x + I_z$, where the horizontal and vertical action variables I_x and I_z are equal to half the Courant-Snyder invariants. The term $D(I)$ is called the diffusion coefficient. It is related to the squared action change per unit time by[4]

$$D(I) = \frac{1}{2}\left\langle \frac{\overline{(\Delta I)^2}}{\Delta t} \right\rangle, \tag{2}$$

while the mean action growth rate $< \overline{\Delta I} > /\Delta t$ is given by

$$\left\langle \frac{\overline{\Delta I}}{\Delta t} \right\rangle = \frac{d}{dI} D(I). \tag{3}$$

Here, the bar indicates the mean over a particle ensemble, and square brackets denote an average over macroscopic regions of phase space.

Note that the diffusion coefficient $D(I)$, as defined by Eq. (2), is not necessarily a monotonous or a smooth function.[5,6]

2.2 Dynamic Aperture and Diffusion Coefficient

The dynamic aperture is the border in phase space inside which particles are stable for a certain large number of turns around the storage ring. It typically corresponds to an action value I_{da} for which the diffusion coefficient is about

$$D(I_{\mathrm{da}}) \approx 10^{-3} I_{\mathrm{da}}^2 \mathrm{s}^{-1}. \tag{4}$$

The dynamic aperture is only well-defined, if, furthermore, the diffusion coefficient increases steeply as a function of amplitude

$$\frac{dD}{dI}(I_{\mathrm{da}}) \cdot \frac{I_{\mathrm{da}}}{D} \gg 1. \tag{5}$$

2.3 Local Diffusion Rates

Several mechanisms have been proposed to explain the transverse particle diffusion in storage rings. Among these mechanisms are Arnold diffusion,[7,8] modulational diffusion,[9,8] resonance streaming,[10,11] and the strong diffusion across the chaotic layer,[12,13] which, in the presence of tune modulation, is formed around the separatrix of each resonance. Predicted diffusion rates for all these processes have been confirmed in simulation studies of simple Hamiltonian systems, which approximately represent the motion in the vicinity of a resonance. In all cases the motion can be locally described by a Fokker-Planck equation in some action variable.[7,8,9,4] Here, dependent on the specific process, 'local' either means inside the chaotic layer or close to a resonance island. If the motion is Hamiltonian the Fokker-Planck equation reduces to a diffusion equation with an action-dependent coefficient.[8,4] We will now introduce the different diffusion mechanisms.

2.3.1 Modulational Diffusion For small modulation frequencies Q_m and large modulation amplitudes q, tune modulation causes a strongly chaotic band of overlapping sideband resonances. Under the influence of a second resonance, particles inside such a modulational layer are driven *along* the resonance contour (compare Fig. 1) and may reach large amplitudes.

More specifically, close to a single resonance, $kQ_x + lQ_z \approx p$, the transverse particle motion is described by the Hamiltonian of Eq. (70), from which it follows that a tune modulation of frequency Q_m and amplitude q (both given in units of the revolution frequency f_{rev}) generates a set of sideband resonances

$$kQ_x + lQ_z + iQ_m - p = 0 \quad (i \neq 0) \tag{6}$$

around the primary resonance ($i = 0$). In the $\bar{I}_x$-$\bar{I}_z$-plane, defined by Eq. (77), two adjacent sideband resonances are separated by a distance $\delta\bar{I}_x$

$$\delta\bar{I}_x \approx \frac{Q_m}{\left|\partial^2\bar{g}/\partial\bar{I}_x^2\right|} = \frac{Q_m}{|l^2\frac{\partial^2 g}{\partial I_z^2} + 2kl\frac{\partial^2 g}{\partial I_x \partial I_z} + k^2\frac{\partial^2 g}{\partial I_x^2}|} \tag{7}$$

and the width of the i-th sideband resonance (in the original I_x-I_z-plane) is[4,14]

$$\Delta I_{\rm tot}^i = \Delta I_{\rm tot}\left|J_i\left(\frac{|l+k|q}{Q_m}\right)\right|^{\frac{1}{2}} \tag{8}$$

where J_i denotes the Bessel function of i-th order, and $\Delta I_{\rm tot}$ is defined in Eq. (85).

A necessary condition for modulational diffusion is the overlap of several (at least two) sideband resonances giving rise to a *modulational layer*. Since the Bessel functions have a significant value only for arguments larger than their order,

$$\lambda \equiv |k+l|q/Q_m \geq i, \tag{9}$$

the maximum number of sideband resonances which may overlap is about

$$R \equiv 2\lambda + 1, \tag{10}$$

assuming λ sidebands on either side of the fundamental resonance.

For relatively small modulation amplitudes—when only the first order sidebands and the fundamental resonance are important ($\lambda \approx 1$)—the resonance-overlap condition[7] can be written as

$$\frac{\Delta\bar{I}_{x,\rm tot}}{\delta\bar{I}_x} \equiv \left[\left|J_0\left(\frac{(k+l)q}{Q_m}\right)\right|^{\frac{1}{2}} + \left|J_{\pm 1}\left(\frac{(k+l)q}{Q_m}\right)\right|^{\frac{1}{2}}\right]\frac{Q_I}{Q_m}2 \geq 1, \tag{11}$$

using the island tune Q_I of Eq. (86). For larger modulation amplitudes (or smaller modulation frequencies) several sidebands can overlap. In this case it is convenient

to approximate the Bessel functions of Eq. (8) by their rms values for large arguments $J_i(\lambda) \approx 1/\sqrt{\pi\lambda}$, (for $\lambda > i$). The overlap condition for the first λ sidebands is then approximately[14,4]

$$\frac{\Delta\bar{I}_{x,\mathrm{tot}}}{\delta\bar{I}_x} \equiv \frac{4}{\pi^{\frac{1}{4}}} \frac{Q_I}{|k+l|^{\frac{1}{4}}\ q^{\frac{1}{4}} Q_m^{\frac{3}{4}}} \geq 1 \tag{12}$$

and, if inequality (11) or (12) is satisfied, the total width $\Delta\bar{I}_{\mathrm{mod}}$ of overlapping resonances in the $\bar{I}_x$-$\bar{I}_z$ plane is given by

$$\Delta\bar{I}_{\mathrm{mod}} = \frac{(2\lambda+1)Q_m}{\left[k^2 \frac{\partial^2 g}{\partial I_x^2} + 2kl \frac{\partial^2 g}{\partial I_x I_z} + l^2 \frac{\partial^2 g}{\partial I_z^2}\right]} \tag{13}$$

which corresponds to

$$\Delta I_{\mathrm{mod}} = \sqrt{k^2+l^2}\Delta\bar{I}_{\mathrm{mod}} \tag{14}$$

when projected onto the diagonal in the I_x-I_z plane.

Provided that there is at least one significant sideband ($\lambda \geq 1$) and that inequality (11) or (12) is fulfilled, modulational diffusion is possible.[9,8] The resulting local diffusion coefficient $D_{\mathrm{mod,\ local}}(I)$ is derived in APPENDIX B.1 for the special case in which the driving resonance is the main coupling resonance $Q_x - Q_z = m$ (m integer),

$$h_{\mathrm{coupl}}(I_x, I_z) = \kappa I_x^{\frac{1}{2}} I_z^{\frac{1}{2}} \cos(\phi_x - \phi_z - m\theta + \chi_0), \tag{15}$$

the parameter κ corresponding to the minimum distance of the measured tunes as a function of nominal tunes.[15] The calculation of the diffusion coefficient involves an average over the modulational layer, since a particle samples all action values inside that layer.

2.3.2 Sweeping Diffusion If the frequency Q_m of the tune modulation is relatively large or the modulation amplitude q small, there is no overlap of strong sidebands, but the tune modulation still gives rise to a stochastic layer of width ΔI_{sl} in the vicinity of the separatrix of a resonance.[7] The relative width $w_{\mathrm{sl}} \equiv \Delta I_{\mathrm{sl}}/\Delta I_{\mathrm{tot}}$ of this stochastic layer may be calculated from an approximate description of motion

close to the separatrix[7,8] and, within a factor of 2, is given by[4]

$$w_{\rm sl} = \frac{\pi|k+l|\ qQ_m^2}{2Q_I^3 \cosh\left(\frac{\pi Q_m}{2Q_I}\right)}. \tag{16}$$

At a constant modulation amplitude q, the width $w_{\rm sl}$ is maximum, when the modulation frequency is of the order of the island tune Q_I. It falls off exponentially $w \sim \exp(-\pi Q_m/(2Q_I))$ for high-frequency modulation ($Q_m \gg Q_I$).

The diffusion rate across the chaotic layer can be derived following Schoch[16] and Evans.[12,13] The change of the action variable for a single crossing of the resonance is calculated by integrating the equations of motion,

$$\begin{aligned}\Delta\bar{I}_{x,\rm single} &\equiv |\bar{I}_{x,2} - \bar{I}_{x,1}| \approx h(I_{x,r}, I_{z,r}) \int_{\theta_1}^{\theta_2} \sin\bar{\phi}_x\ d\theta \\ &\approx h(I_{x,r}, I_{z,r}) \left[\sin\bar{\phi}_{x,0} \int_{\theta_1}^{\theta_2} \cos\left(\frac{\bar{\phi}''_{x,0}}{2}(\theta-\theta_0)^2\right)\ d\theta + \right. \\ &\quad \left. + \cos\bar{\phi}_{x,0} \int_{\theta_1}^{\theta_2} \sin\left(\frac{\bar{\phi}''_{x,0}}{2}(\theta-\theta_0)^2\right)\ d\theta\right]. \end{aligned} \tag{17}$$

Here, a second order Taylor expansion has been performed around the stationary phase $\bar{\phi}_{x,0}$, at which $\bar{\phi}'_{x,0} \equiv d\bar{\phi}_x/d\theta\ |_{\theta=\theta_0} = 0$. If the intervals $|\theta_1 - \theta_0|$ and $|\theta_2 - \theta_0| \gg 0$ are sufficiently large,[16] we are left with the evaluation of two Fresnel integrals. Averaging the absolute value of $\Delta\bar{I}_{x,\rm single}$ (17) over the phase $\bar{\phi}_{x,0}$ then yields

$$\Delta\bar{I}_{x,\rm single} = h(I_{x,r}, I_{z,r})\sqrt{\frac{8}{\pi|\bar{\phi}''_{x,0}|}}. \tag{18}$$

If between successive resonance crossings the phase correlation of different particles is lost, the mean squared change of the action can be calculated as an incoherent sum of single resonance crossings. After N resonance crossings we expect

$$\overline{(\Delta\bar{I}_x)^2} = N(\Delta\bar{I}_{x,\rm single})^2. \tag{19}$$

Remembering now, that the resonance crossing is due to the tune modulation, the modulus of the second derivative of the phase is replaced by its average value

$$|\bar{\phi}''_{x,0}| \approx \frac{2}{\pi} qQ_m \tag{20}$$

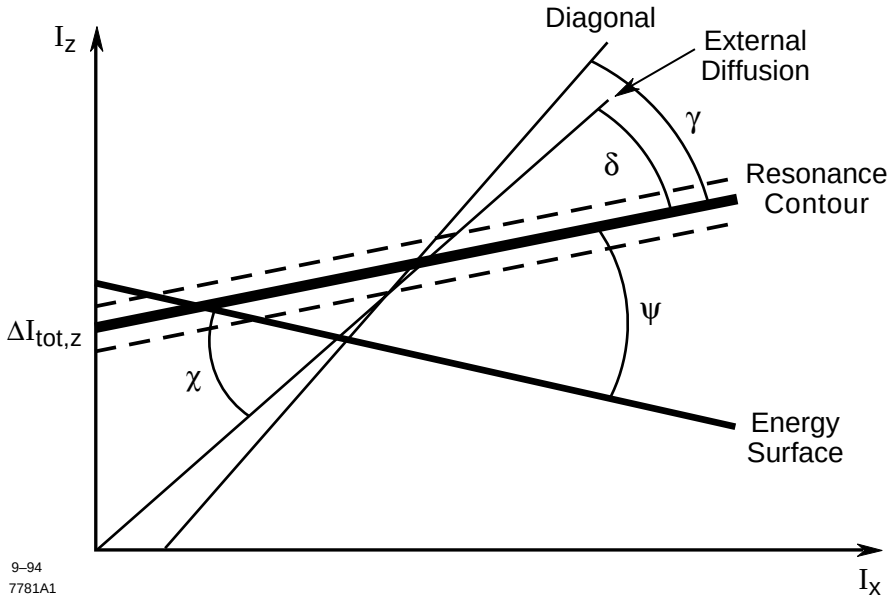

FIGURE 1: Schematic view of energy surface and resonance contours in the I_x-I_z plane, along with the direction of the external diffusion (for instance due to gas scattering). The angles between the four directions are used in Eqs. (24)–(30).

and the expression for the local action growth becomes

$$D_{\text{sd, local}}(I) \equiv \frac{\overline{(\Delta I)^2}}{2\Delta t} = 4\frac{f_{rev}|k+l|h^2(I_{x,r}, I_{z,r})}{q}, \tag{21}$$

where $I \equiv I_x + I_z$ denotes the total transverse action. Equation (21) agrees well with simulation results for a two-dimensional map.[4]

2.3.3 Resonance Streaming Another diffusion mechanism is resonance streaming.[10,11] The effect of an externally generated diffusion ('noise', for instance gas scattering), characterized by a diffusion coefficient $D_{\text{ext}}(I)$, may be considerably increased in the vicinity of a resonance. Roughly speaking, for this diffusion enhancement a certain minimum value of island tune and island width is required and the angle in action space between energy surface 'H = constant' and resonance contour (74) has to be small.

Fig. 1 presents a schematic picture of energy surface, resonance contour and external diffusion in the two-dimensional action space. The direction of the energy

surface (H = constant) in the I_x-I_z plane is given by the vector

$$\begin{pmatrix} I_x \\ I_z \end{pmatrix}_{\text{energy}} = \begin{pmatrix} k \\ l \end{pmatrix} \tag{22}$$

while the tangent vector to the resonance contour (74) is

$$\begin{pmatrix} I_x \\ I_z \end{pmatrix}_{\text{resonance}} = \begin{pmatrix} l \\ -k\frac{\frac{\partial^2 g}{\partial I_x^2}+\frac{\partial^2 g}{\partial I_x \partial I_z}}{\frac{\partial^2 g}{\partial I_z^2}+\frac{\partial^2 g}{\partial I_x \partial I_z}} \end{pmatrix}. \tag{23}$$

One necessary condition for enhancement of the external diffusion by the resonance is that the angle ψ between the resonance contour and the energy surface is small compared with the angle χ between external diffusion and energy surface:

$$|\sin\psi| < |\sin\chi|. \tag{24}$$

A second condition for resonance streaming is that the average time τ_D after which a particle traverses a distance comparable to the island width under the influence of the external diffusion is large compared with the oscillation period inside the resonance:

$$Q_I f_{rev} \tau_D > 1, \tag{25}$$

where

$$\tau_D \equiv \frac{(\Delta I_{\text{tot,trans}})^2}{2D_{\text{ext,trans}}}. \tag{26}$$

The term $D_{\text{ext,trans}}$ is the component of the external diffusion transverse to the resonance contour,

$$D_{\text{ext,trans}}(I) \equiv D_{\text{ext}}(I)\,\sin^2\delta, \tag{27}$$

where δ is the angle between the resonance contour and the external diffusion, and $\Delta I_{\text{tot,trans}}$ is the corresponding projection of the total island width

$$\Delta I_{\text{tot,trans}} = \Delta I_{\text{tot}}|\sin\psi|. \tag{28}$$

If both conditions (24) and (25) are satisfied, the diffusion *along* the resonance line is enhanced, and is characterized by the diffusion coefficient[10,8]

$$D_{\text{along}}(I) \approx D_{\text{ext}}(I)\frac{\sin^2\chi}{\sin^2\psi}. \tag{29}$$

The diffusion in the total transverse action $I \equiv I_x + I_z$ is obtained by projecting $D_{\rm along}(I)$ onto the diagonal direction

$$D_{\rm res\ str}(I) \approx D_{\rm ext}(I) \frac{\cos^2\gamma \sin^2\chi}{\sin^2\psi} \tag{30}$$

where γ is the angle between the diagonal vector in the I_x-I_z plane $(I_x, I_z)_{\rm diag} \equiv (1,1)$ and the resonance contour.

According to Tennyson,[10] even if condition (25) is violated, diffusion enhancement is still possible, as long as the motion induced by the resonance is faster than the external diffusion. In this 'plateau regime,'[10] defined by the two inequalities

$$1 \quad > \quad \tau_D Q_I f_{rev} \qquad \text{and} \tag{31}$$

$$2\pi f_{rev} \tau_D \sqrt{2}|k+l|h \quad > \quad \Delta I_{\rm tot,trans}, \tag{32}$$

a particle typically stays inside the resonance island for less than a resonance libration period.

2.3.4 Arnold Diffusion As discussed in Sections 2.3.1 and 2.3.2, if the modulation frequency Q_m is large or the modulation amplitude q small, no modulational layer of overlapping sideband resonances is formed, but the tune modulation still generates a stochastic layer around the separatrix of each fundamental resonance. Under the influence of a second resonance, particles inside this stochastic layer may diffuse *along* the primary resonance contour, which is an example of Arnold diffusion.[7,8] The process is similar to the modulational diffusion, but the chaotic regions are much smaller and so are the diffusion rates. The corresponding diffusion coefficient is computed in APPENDIX B.2, supposing, as in the treatment of modulational diffusion, that the driving term of the main coupling resonance $Q_x - Q_z = m$, Eq. (15), causes the diffusion along the stochastic layer.

2.4 Averaging and Macroscopic Diffusion Coefficients

Beam lifetime and dynamic aperture are determined by the 'macroscopic' diffusion over regions of phase space that are large compared with a resonance island. A

simple way of approximating the macroscopic diffusion coefficient $D(I)$ of Eq. (1) consists in averaging the local diffusion coefficient, due to one of the processes discussed in the previous section, over the (regular and chaotic) regions between two adjacent resonance islands.

The motivation for this average is drifts of the storage ring parameters: the parameters in the Hamiltonian (70), such as the linear tunes Q_{x0} and Q_{z0}, the detuning term g and the resonance-driving term h, undergo continuous small variations due to low-frequency quadrupole vibrations, decay of persistent currents in the superconducting magnets, and temperature changes of magnets and power supplies. Associated with these changes is a drift of the position of resonance islands and chaotic regions in phase space. Denoting the mean change of the tunes per unit time by $\dot{Q}_0$, the rate at which the position of a resonance island varies is about

$$\left|\frac{\Delta I}{\Delta t}\right|_{\text{drift}} \approx \frac{(k^2+l^2)\dot{Q}_0}{|\partial^2\bar{g}/\partial\bar{I}_x^2|}. \tag{33}$$

The drifts in the horizontal and vertical directions are of similar magnitude.

The global diffusion coefficient can be approximated by a macroscopic average of the local coefficients, if the following conditions are satisfied:

1. Over a certain time period Δt_{drift}, whose value depends on the specific aperture measurement, the island positions have to change at least by a distance ΔI_{drift} which is comparable to the separation $\delta I \approx (k^2+l^2)/(\tilde{m}^3\frac{\partial^2\bar{g}}{\partial\bar{I}_x^2})$ of two adjacent resonances through order $\tilde{m}$:

$$|\Delta I|_{\text{drift}} \geq \frac{1}{\tilde{m}^3}\frac{(k^2+l^2)}{\left|k^2\frac{\partial^2 g}{\partial I_x^2}+2kl\frac{\partial^2 g}{\partial I_x I_z}+l^2\frac{\partial^2 g}{\partial I_z^2}\right|}, \tag{34}$$

   where $\tilde{m}$ denotes the maximum resonance order which is still significant (for instance, the resonances of which order still occupy a certain area in phase space). This implies

$$\left|\frac{\Delta I}{\Delta t}\right|_{\text{drift}} \geq \frac{(k^2+l^2)}{\tilde{m}^3}\frac{1}{\left|k^2\frac{\partial^2 g}{\partial I_x^2}+2kl\frac{\partial^2 g}{\partial I_x I_z}+l^2\frac{\partial^2 g}{\partial I_z^2}\right|}\frac{1}{\Delta t_{\text{drift}}}. \tag{35}$$

2. The drift has to be fast compared with the motion inside the stochastic layer, inside the modulational layer or in the resonance island for, respectively, sweep-

ing diffusion, modulational diffusion, and resonance streaming. This translates roughly into the conditions

$$\left|\frac{\Delta I}{\Delta t}\right|_{\text{drift}} \gg \frac{2\pi Q_I f_{rev} \Delta I_{\text{tot}}}{\ln\left(\frac{32\ e}{w_{\text{sl}}}\right)} \quad \text{(for sweeping and Arnold diffusion)} \tag{36}$$

$$\left|\frac{\Delta I}{\Delta t}\right|_{\text{drift}} \gg 2\pi f_{rev}\ n\ h \quad \text{(for modulational diffusion)} \tag{37}$$

$$\left|\frac{\Delta I}{\Delta t}\right|_{\text{drift}} \gg 4\pi f_{rev} Q_I\ \Delta I_{\text{tot}} \quad \text{(for resonance streaming)}, \tag{38}$$

where $\frac{1}{2\pi Q_I f_{rev}} \ln\left(\frac{32e}{w_{\text{sl}}}\right)$ is the average half period of oscillation inside the chaotic layer and $n \equiv \min(|k|, |l|)$. If the parameter drift fulfills any of the inequalities (36) through (38), the corresponding local diffusion is adiabatic with respect to the parameter drifts, and particles cannot be trapped by passing chaotic layers or passing resonance islands. This is also always the case when the drift contains a discontinuous, step-like component.

3. Simultaneously, however, the parameter variations have to be slow compared with the tune modulation:

$$\left|\frac{\Delta I}{\Delta t}\right|_{\text{drift}} \ll \frac{2\pi q Q_m f_{rev}(k^2 + l^2)}{\left|k^2 \frac{\partial^2 g}{\partial I_x^2} + 2kl \frac{\partial^2 g}{\partial I_x I_z} + l^2 \frac{\partial^2 g}{\partial I_z^2}\right|}. \tag{39}$$

Only if inequality (39) is satisfied, does the Hamiltonian (70) provide an adequate description of the dynamics over several tune modulation periods.

4. In the case of sweeping diffusion, moreover, the island drift rate has to be larger than the mean local action growth rate predicted from the local diffusion coefficient:

$$\left|\frac{\Delta I}{\Delta t}\right|_{\text{drift}} \gg \frac{dD_{\text{sd, local}}}{dI} \qquad \text{(for sweeping diffusion)}. \tag{40}$$

Otherwise the averaged diffusion coefficient gives an overestimate of the actual diffusion.

Provided that the conditions (34), (37), and (39) are fulfilled, the 'macroscopic' diffusion coefficient due to modulational diffusion at the position of the ith resonance may be obtained by averaging the local coefficients $D_{\text{mod, local}}$, Eqs. (101),

(102), or (104), over the region between two resonances:

$$D_{\rm mod}(I_i) \approx \frac{\Delta I_{{\rm mod},i}}{\delta I_i} D_{{\rm mod,\ local},i}(I_i) \tag{41}$$

where δI_i is the sum of the half-distances to the two adjacent resonances $\delta I_i \equiv (I_{i+1} - I_{i-1})/2$, and $\Delta I_{{\rm mod},i}$ (Eq. (14)) is the width of the modulational layer along the diagonal direction in the I_x-I_z plane. If the width of the modulational layer is of the same order of magnitude as the separation between two adjacent primary resonances, i.e., if $\Delta I_{{\rm mod},i} \approx \delta I_i$, Eq. (41) simplifies to

$$D_{\rm mod}(I_i) \approx D_{{\rm mod,\ local},i}(I_i). \tag{42}$$

In this case the local and macroscopic diffusion coefficients are identical.

If (34), (36), (39), and (40) are fulfilled, the diffusion across the chaotic layer, Eq. (21), in conjunction with a drift of the machine parameters gives rise to a macroscopic diffusion, which may be called 'sweeping diffusion' and whose diffusion coefficient reads

$$D_{\rm sd}(I_i) = \frac{1}{2} \left\langle \frac{\overline{(\Delta I)^2}}{\Delta t} \right\rangle_i \approx \frac{\Delta I^i_{\rm tot} \cdot w_{{\rm sl},i}}{\delta I_i} \cdot D_{{\rm sd,\ local},i}(I_i), \tag{43}$$

which again follows from averaging a local rate (Eq. (21)) over the region between two resonances. The diffusion coefficient of Eq. (43) is independent of the modulation amplitude q, since the fraction of phase space covered with chaotic trajectories increases linearly with the modulation amplitude q, whereas the diffusion rate in this zone decreases as $1/q$ (see Eqs. (16) and (21)).

In an analogous way estimates of macroscopic diffusion coefficients can be obtained for resonance streaming and for Arnold diffusion.

2.5 Extrapolation to Higher Resonance Orders

Parameters of resonances can only be calculated up to a certain order, which arises either from divergences due to small denominators or from the limited computing power. It is, however, possible to use scaling laws for extrapolating certain quantities to higher orders, since the resonance-driving terms $h_{\tilde{m}}$ of order $\tilde{m} \equiv |k| + |l|$

will roughly scale as

$$h_{\tilde{m}} \propto (aI)^{\frac{\tilde{m}}{2}}. \tag{44}$$

If the storage ring is represented by a Taylor map, for instance, by using differential algebra,[17] the value of the coefficient a can be estimated from the magnitude of the Taylor map coefficients as a function of order $\tilde{m}$. From Eq. (44) it follows that

$$\frac{\Delta I_{\text{tot},\ \tilde{m}}}{\Delta I_{\text{tot},\ \tilde{m}-1}} \approx (aI)^{\frac{1}{4}} \tag{45}$$

$$\frac{Q_{I,\ \tilde{m}}}{Q_{I,\ \tilde{m}-1}} \approx (aI)^{\frac{1}{4}}. \tag{46}$$

and the distance $\delta I_{\tilde{m}}$ between two adjacent resonances through order $\tilde{m}$ scales approximately as

$$\delta I_{\tilde{m}} \propto \frac{1}{\tilde{m}^3}. \tag{47}$$

In the I_x-I_z plane, the resonance islands of order $\tilde{m}$ cover a total area which is roughly proportional to

$$\sum_i \Delta I_{\text{tot},\tilde{m},i}(I) \approx \tilde{m}^2 e^{\frac{\tilde{m}}{4}\ln(aI)}, \tag{48}$$

where the subindex i denotes the individual resonances of order $\tilde{m}$. The maximum area is occupied by resonances of order

$$\tilde{m}_{\max}(I) \approx -\frac{8}{\ln(aI)}. \tag{49}$$

Note that the order $\tilde{m}_{\max}$ is action-dependent and increases for large action values.

The inverse of a is an upper limit for the dynamic aperture, $I_{\text{da}} < \frac{1}{a}$, since for $I \geq \frac{1}{a}$ the series

$$\sum_{\tilde{m}} \sum_i \Delta I_{\text{tot},\tilde{m},i}(I), \tag{50}$$

characterizing the total area covered by resonance islands of all orders, does not converge and, therefore, strong resonance overlap is expected.

3 APPLICATION TO HERA

3.1 Introduction

In this section, the semi-analytical scheme developed above is used to calculate macroscopic diffusion rates for the HERA proton ring at DESY, which is the second superconducting storage ring in operation. The single-particle beam dynamics in HERA is similar to that envisioned for the proposed Large Hadron Collider (LHC) at CERN. Note, in particular, that the ratio of luminosity energy and injection energy, which partly determines the field quality of the s.c. magnets at injection, is about a factor of 20 both for HERA and for the LHC compared with a ratio of only 6 for the Fermilab Tevatron. A description of simulation studies and aperture measurements at HERA is presented in APPENDIX C. Here, it shall only be mentioned that the dynamic aperture, as deduced from beam profile measurements after bad injection or excitation, is of the order

$$I_{\mathrm{da}}^{\mathrm{measured}} \approx 0.5 - 0.8 \text{ mm mrad}, \tag{51}$$

where the uncertainty refers to variations observed over periods of several days.

3.2 Tune Modulation and Parameter Drifts

In the HERA proton ring several sources of tune modulation and of parameter drifts exist. Their order of magnitude and frequency range will now be estimated.

3.2.1 Tune Modulation due to Power Supply Ripple and Synchrotron Oscillations

Current ripple in the superconducting main circuit causes a tune modulation of frequency 50 Hz ($Q_m \approx 10^{-3}$) and of amplitude $q \approx 5 \cdot 10^{-5}$.[4]

Also the effect of synchrotron motion and nonzero chromaticity may to first order be approximated by the accompanying tune modulation in the transverse phase space. Here, assuming a relative energy deviation $\delta \approx 2 \cdot 10^{-4}$ and a chromaticity $\xi \equiv \Delta Q / \frac{\Delta p}{p} \approx 1$, a typical modulation amplitude is $q \approx 2 \cdot 10^{-4}$. The synchrotron frequency of about 20 Hz corresponds to $Q_m \approx 4 \cdot 10^{-4}$.

3.2.2 Spread of Persistent-Current Decay Over thirty minutes the spread of decay of the persistent current sextupole components is of the order $\Delta b_{3,\mathrm{rms}} = 2 \cdot 10^{-4}$ (at a reference radius $r_0 = 25$ mm).[18] It causes a change of the detuning $\partial^2 g / \partial I_x^2$ by roughly

$$\Delta \left(\frac{\partial^2 g}{\partial I_x^2} \right) \approx \frac{N_{\mathrm{mag}}}{32\pi} (\Delta b_{3,\mathrm{rms}})^2 \frac{\theta_{\mathrm{dip.}}^2}{r_0^4} < \beta_x^3 > \left[\frac{3}{\sin \pi Q_x} + \frac{1}{\sin 3\pi Q_x} \right] \mathrm{m}^{-1} \quad (52)$$

$$\approx 2 \cdot 10^2 \ \mathrm{m}^{-1} \quad (53)$$

where $N_{\mathrm{mag}} \approx 400$ denotes the number of dipole magnets, $\theta_{\mathrm{dip.}} \approx 15$ mrad the dipole bending angle, $Q_x \approx 0.3$ the horizontal tune, and $< \beta_x^3 >^{\frac{1}{3}} \approx 60$ m the horizontal beta function. Similar expressions and values apply for the other second order partial derivatives with respect to I_x and I_z of the detuning function g. At an amplitude $I \approx 1$ mm mrad equation (53) predicts a tune change per unit time of about

$$\dot{Q}_{0,x}^{\mathrm{p.c.d.}} \approx 10^{-7} \ \mathrm{s}^{-1}. \quad (54)$$

3.2.3 Ground Motion Effects Ground waves plus mechanical vibrations of the magnets and the associated orbit changes in the sextupole fields cause a low-frequency tune variation. The typical frequency range of these effects is 2–20 Hz ($Q_m^{\mathrm{g.m.}} \approx 10^{-4}$) and the amplitude of the tune change is of the order of $q^{\mathrm{g.m.}} \approx 10^{-6}$ [19,4].

3.2.4 Slow Tune Drift A slow drift by typically $\dot{Q}_0^{\mathrm{temp}} \approx 10^{-4}$ hr^{-1} is ascribed to temperature changes of magnets and power supplies.

3.3 Resonance Parameters and Extrapolation to Higher Order

For a detailed model of HERA and for three different working points a normal-form analysis has been performed, providing parameters of resonances through order 11 (compiled in APPENDIX D). The magnitude of typical resonance-driving terms h for even higher orders may be obtained by extrapolation as discussed in Section 2.5. From a four-dimensional Taylor map representing the HERA proton

ring, one estimates the value

$$a \approx 0.38 \tag{55}$$

for the scaling parameter a defined in Eq. (44) (compare also the six-dimensional result in Kleiss[20]). Thus, at $I \approx 1$ mm mrad the maximum area in phase space is occupied by resonances of order $\tilde{m}_{\max} \approx 8$, from Eq. (49), while for resonance islands of order $\tilde{m} \approx 29$ the total area covered is comparable to that covered by the first order resonances. Moreover, the value $1/a \approx 2.6$ mm mrad constitutes an upper limit for the dynamic aperture (see Section 2.5).

3.4 Applicability of Averaging

The total drift rate of resonance islands in phase space is given by the sum of at least three different contributions, ground motion, persistent-current decay, and temperature changes:

$$\left(\frac{\Delta I}{\Delta t}\right)_{\text{drift}} \approx \left(\frac{\Delta I}{\Delta t}\right)_{\text{ground motion}} + \left(\frac{\Delta I}{\Delta t}\right)_{\text{p.c. decay}} + \left(\frac{\Delta I}{\Delta t}\right)_{\text{temperature}} . \tag{56}$$

The magnitude of each contribution may be estimated from the quoted drift parameters using Eq. (33):

$$\left|\frac{\Delta I}{\Delta t}\right|_{\text{ground motion}} \approx \frac{2\pi q^{\text{g.m.}} Q_m^{\text{g.m.}} f_{rev}(k^2+l^2)}{|\partial^2 \bar{g}/\partial I_x^2|} \approx 10^{-2} \text{ mm mrad s}^{-1} \tag{57}$$

$$\left|\frac{\Delta I}{\Delta t}\right|_{\text{p.c. decay}} \approx \max\left(\frac{\dot{Q}_{0,x}^{\text{p.c.d.}}}{\partial^2 g/\partial I_x^2}, \frac{\dot{Q}_{0,z}^{\text{p.c.d.}}}{\partial^2 g/\partial I_z^2}\right) \approx 3.5 \cdot 10^{-4} \text{ mm mrad s}^{-1} \tag{58}$$

$$\left|\frac{\Delta I}{\Delta t}\right|_{\text{temperature}} \approx \frac{(k^2+l^2)\dot{Q}_0^{\text{temp}}}{|\partial^2 \bar{g}/\partial I_x^2|} \approx 10^{-5} \text{ mm mrad s}^{-1} \tag{59}$$

After a time Δt_{drift} the persistent-current decay gives rise to an absolute change of resonance positions in phase space by

$$|\Delta I|_{\text{drift}} \approx \Delta t_{\text{drift}} \cdot \left|\frac{\Delta I}{\Delta t}\right|_{\text{p.c. decay}} \approx \Delta t_{\text{drift}} \cdot 3.5 \cdot 10^{-4} \text{ mm mrad s}^{-1}. \tag{60}$$

For instance, if one assumes a maximum resonance order $\tilde{m} \approx 29$, two adjacent resonances are separated by $\delta I \equiv (k^2+l^2)/(\tilde{m}^3 \frac{\partial^2 \bar{g}}{\partial I_x^2}) \approx 0.014$ mm mrad and, hence, in this case the condition (34) is fulfilled for $\Delta t_{\text{drift}} > 40$ s.

The typical velocities inside the stochastic or modulational layer or inside a resonance island are

$$\frac{2\pi Q_I f_{rev} \Delta I_{\rm tot}}{\ln(\frac{32\ e}{w_{\rm sl}})} \approx \begin{cases} 1.6 \cdot 10^{-7} \text{ mm mrad s}^{-1} & \text{(for p.s. ripple)} \\ 4 \cdot 10^{-7} \text{ mm mrad s}^{-1} & \text{(for sync. oscillations)} \end{cases} \tag{61}$$

$$2\pi f_{rev}\ nh \approx 2.6 \cdot 10^{-7} \text{ mm mrad s}^{-1} \tag{62}$$

$$4\pi f_{rev} Q_I\ \Delta I_{\rm tot} \approx 8 \cdot 10^{-6} \text{ mm mrad s}^{-1}, \tag{63}$$

where the numerical values on the right-hand side are the geometric means for the set of resonances listed in the appendix. In case of Eq. (61) only those resonances are taken into account for which the stochastic width $w_{\rm sl}$ is non-negligible. Comparison of the drift rates, Eqs. (57)–(59), with Eqs. (61)–(63) shows that conditions (36)–(38) are satisfied.

Finally, inequality (39) evaluates to

$$\left|\frac{\Delta I}{\Delta t}\right|_{\rm drift} \ll \frac{2\pi q Q_m f_{rev}(k^2+l^2)}{\left|k^2 \frac{\partial^2 g}{\partial I_x^2} + 2kl \frac{\partial^2 g}{\partial I_x I_z} + l^2 \frac{\partial^2 g}{\partial I_z^2}\right|} \approx 8.4 \text{ mm mrad s}^{-1}, \tag{64}$$

again quoting the geometric mean over all resonances, and is also fulfilled for all three types of parameter drifts.

3.5 Width of Resonance Islands and Chaotic Layers

Fig. 2 shows the island width $\Delta I_{\rm tot}$ for our set of resonances through order 11 (listed in APPENDIX D). The resonances represented in the picture are encountered for different working points and along different lines in tune space.

The island tune for the resonances varies between $3 \cdot 10^{-15}$ (10^{-10} Hz) at very small amplitudes and $5 \cdot 10^{-4}$ (25 Hz) for amplitudes of about 23 mm ($\beta = 76$ m).[4] Resonance islands are most sensitive to an external tune modulation at frequencies close to the island frequency. In contrast, they are almost undisturbed by high-frequency perturbations (i.e., $f > 100$ Hz).

In Fig. 3 the absolute width of the chaotic layer $w_{\rm sl}\Delta I_{\rm tot}$ as caused by power supply ripple is depicted for each resonance, again as a function of the action I. Comparison with Fig. 2 shows that up to 10% of a resonance island can become

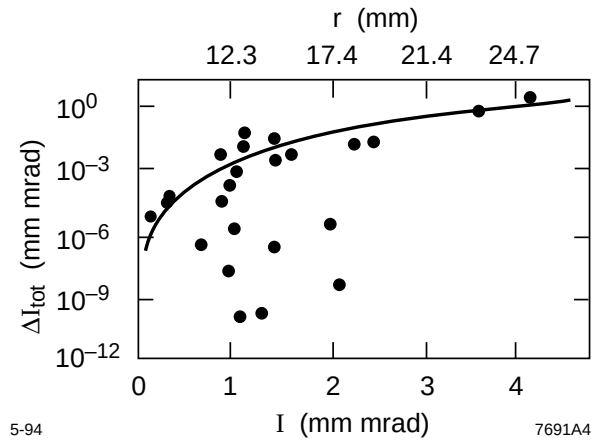

FIGURE 2: Total island width $\Delta I_{\rm tot}$ as a function of the resonant action $I \equiv I_x + I_z$, for the resonances listed in APPENDIX D (dots). The curve represents the parametrization $\Delta I_{\rm tot} \approx 2.4 \cdot 10^{-3} I^4 (\text{mm mrad})^{-3}$. The amplitude r of the upper horizontal axis is defined by $r \equiv (2\beta(I_x + I_z))^{\frac{1}{2}}$ with the typical beta function $\beta = 76$ m.

chaotic. For about half of the resonances of Fig. 2, however, the stochastic width $w_{\rm sl}$ is insignificant. In particular, it is negligibly small at resonant action values below $I_0 \approx 0.8$ mm mrad ($r \approx 11$ mm). This I_0 approximates the threshold for tune-modulation induced sweeping or Arnold diffusion, and its value is in remarkable agreement with the dynamic acceptance measured (Eq. (51)).

3.6 Modulational Diffusion

If the tune modulation is caused by power supply ripple (see subsection 3.2.1), at most the two first order sideband resonances may become sizable, according to Eq. (9). In this case, the overlap condition, Eq. (11), translates into

$$Q_I \geq 3.4 \cdot 10^{-4}. \tag{65}$$

Fig. 4a shows the expression on the left hand side of Eq. (11) plotted as a function of the resonant action value. The overlap condition is fulfilled and, hence, modulational layers are generated only for the outermost resonances. There are several resonances at action values between $I \approx 1$ mm mrad and $I \approx 4$ mm mrad for which

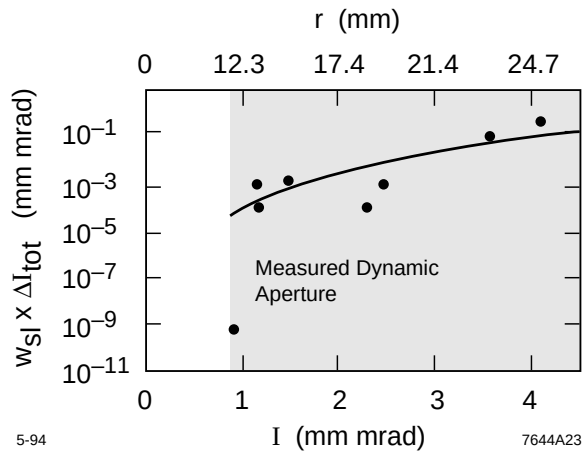

FIGURE 3: Absolute width of stochastic layer $\Delta I_{\rm tot} \cdot w_{\rm sl}$ as a function of the resonant action $I \equiv I_x + I_z$, for the resonances listed in APPENDIX D (dots). A tune modulation amplitude of $q \approx 5 \cdot 10^{-5}$ at a frequency $Q_m \approx 10^{-3}$ is assumed. The curve represents the parametrization $w_{\rm sl} \cdot \Delta I_{\rm tot} \approx 10^{-4} I^5 (\text{mm mrad})^{-4}$. The amplitude r of the upper horizontal axis is defined by $r \equiv (2\beta(I_x + I_z))^{\frac{1}{2}}$ with the typical beta function $\beta = 76$ m.

the sidebands almost overlap (but even for $q = 10^{-4}$ they do not).

In the case of tune modulation due to typical synchrotron oscillations and nonzero chromaticity (subsection 3.2.1), the total number of strong sidebands is of the order 4–12, from Eqs. (9) and (10). The overlap condition, Eq. (12), corresponds to

$$Q_I \geq 1.5 - 2 \cdot 10^{-4}, \tag{66}$$

and, hence, occurs for a smaller value of the island tune Q_I than in the case of power supply ripple. In Fig. 4b the expression on the left hand side of Eq. (12) is depicted as a function of the resonant action value. In this case the overlap condition is fulfilled for about half of the resonances. Note that the sidebands overlap only for action values $I \geq 0.5$ mm mrad, which again is in good agreement with the dynamic aperture measured (see Eq. (51)).

Figs. 5a and b show the total width of the modulational layer $\Delta I_{\rm mod}$, Eq. (14), as caused by power supply ripple and synchrotron oscillations, respectively. In Figs. 5c and d the relative width of the modulational layer $\Delta I_{\rm mod}/\delta I$ is depicted for typical

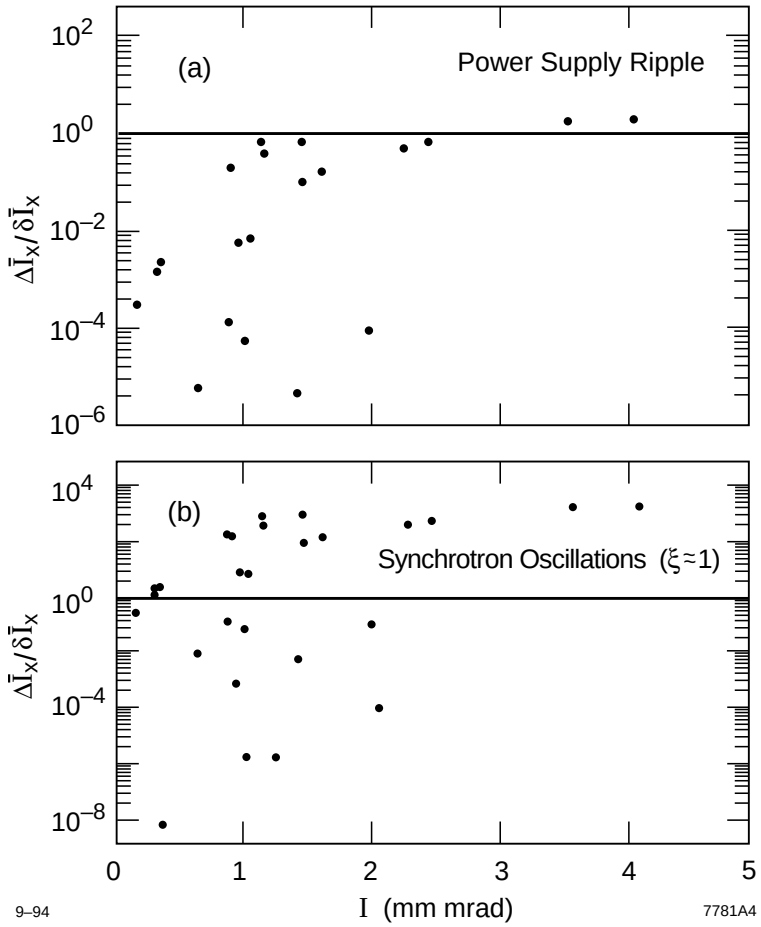

FIGURE 4: Overlap condition $\Delta\bar{I}_x/\delta\bar{I}_x$, Eq. (11) and (12), respectively, as a function of the resonant action, assuming a tune modulation of a) $q \approx 5 \cdot 10^{-5}$ and $Q_m \approx 10^{-3}$ as due to power supply ripple, b) $q \approx 2 \cdot 10^{-4}$ and $Q_m \approx 4 \cdot 10^{-4}$ as due to synchrotron oscillations and nonzero chromaticity ($\xi \approx 1$). For values larger than 1, the sideband resonances overlap and give rise to a modulational layer.

synchrotron oscillations at two different values of chromaticity, namely $\xi \approx 1$ and $\xi \approx 5$; δI being the sum of the half-distances to the two adjacent resonances. In the case of power supply ripple and for well compensated chromaticity, $\xi \leq 1$, adjacent modulational layers do not overlap (Fig. 5c). For larger chromaticity, $\xi \approx 5$, however, the modulational layers are so wide that the regular regions of

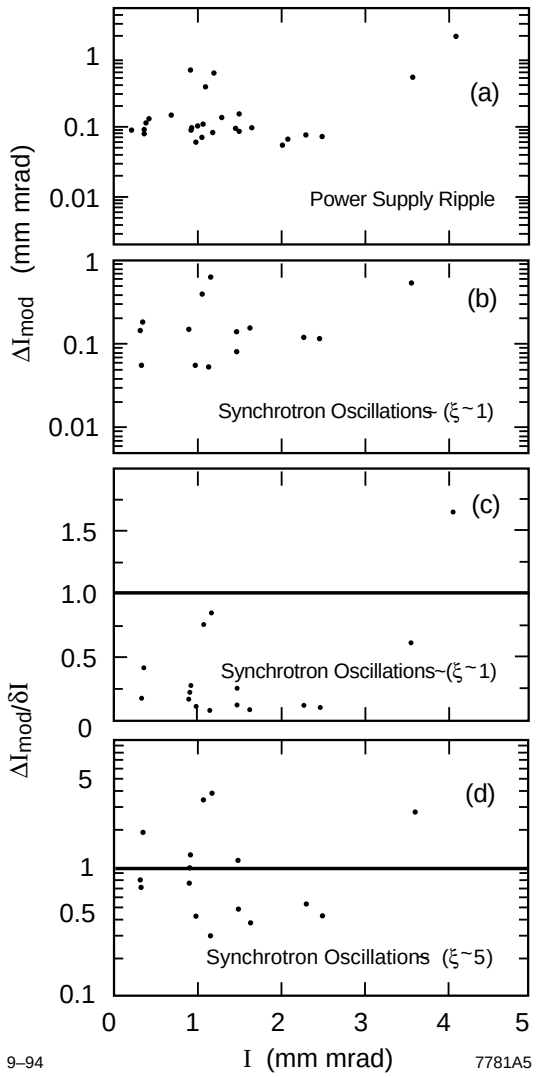

FIGURE 5: Width of modulational layer as a function of the resonant action $I \equiv I_x + I_z$: a) absolute width $\Delta I_{\rm mod}$ due to power supply ripple assuming three overlapping sideband resonances, b) absolute width $\Delta I_{\rm mod}$ in the case of synchrotron oscillations ($q \approx 2 \cdot 10^{-4}$, $Q_m \approx 4 \cdot 10^{-4}$), c) relative width of modulational layer $\Delta I_{\rm mod}/\delta I$ for typical synchrotron oscillations and a corrected chromaticity $\xi \approx 1$ ($q \approx 2 \cdot 10^{-4}$, $Q_m \approx 4 \cdot 10^{-4}$), d) relative width $\Delta I_{\rm mod}/\delta I$ for synchrotron oscillations and a chromaticity $\xi \approx 5$ ($q \approx 10^{-3}$, $Q_m \approx 4 \cdot 10^{-4}$). For values of $\Delta I_{\rm mod}/\delta I$ larger than 1 adjacent modulational layers overlap.

phase space become negligible, as demonstrated by Fig. 5d. In that case most of the particles are chaotic and thus potentially unstable, even if the machine parameters were constant, and the macroscopic diffusion coefficient is approximately equal to the local coefficient (compare Eq. (42)). If resonances through order $\tilde{m} \approx 18$ were to be taken into account, Eq. (42) would also apply for $\xi \approx 1$, since the distance between adjacent resonances scales as $\delta I \propto 1/\tilde{m}^3$.

The diffusion rate, Eq. (41), evaluated for power supply ripple is shown in Fig. 6a for $|Q_{x0} - Q_{z0} - m| \approx 0.005$ and a linear coupling strength $\kappa \approx 0.005$. An overlap of only three sideband islands has been assumed for each resonance, but, as indicated by Fig. 4, even this modest overlap may not occur.

On the other hand, synchrotron oscillations plus nonzero chromaticity generate a larger number of strong sidebands, a significant fraction of which is actually overlapping. The diffusion coefficient $D_{\text{mod.}}(I)$, Eq. (41), for this case is depicted in Fig. 6b, again for $|Q_{x0} - Q_{z0} - m| \approx 0.005$ and assuming a linear coupling strength of $\kappa \approx 0.005$. Here, only resonances are represented for which $|k+l|\ q/Q_m \geq 1$ (i.e., at least the first order sideband resonance is sizable) and for which, furthermore, the overlap criterion, Eq. (12), is fulfilled.

That the rate of modulational diffusion very sensitively depends on the working point is illustrated by Fig. 6c, which shows the maximum diffusion coefficient $D_{\text{mod, local}}(I)$, obtained from Eqs. (104) and (41). It is attained if the working point is set on the coupling resonance $|Q_{x0} - Q_{z0} - m| \approx 0$. Its value is many orders of magnitude larger than those in Fig. 6a and b.

Finally, note that diffusion of particles along the modulational layer can not only be caused by the linear coupling resonance, but also by another high-order resonance. Assuming that the latter is characterized by the driving term $\tilde{h}$, the corresponding diffusion is smaller than the maximum rate calculated for the linear coupling resonance, shown in Fig. 6c, by at least the factor $\tilde{h}^2/(\kappa^2 I_x I_z) \approx 10^{-20}$.

3.7 Sweeping Diffusion

Fig. 7a shows the local action growth rate (21) for our set of resonances through order 11. The averaging condition (40) is fulfilled for, roughly,

$$I \leq 2 \text{ mm mrad} \tag{67}$$

and at least in this amplitude range the macroscopic diffusion coefficient $D_{\rm sd}(I)$ can be calculated according to Eq. (43). It is shown in Fig. 7b assuming a modulation frequency of 50 Hz ($Q_m = 10^{-3}$), as that due to power supply ripple.

3.8 Resonance Streaming

To estimate the diffusion enhancement due to resonance streaming, let us approximate the effect of residual gas scattering by an external diffusion in the diagonal direction, $(I_x, I_z)_{\rm diag} = (1, 1)$, characterized by the diffusion coefficient

$$D_{\rm ext}(I) = \frac{1}{2} < \beta > \left(\frac{14.1 \text{ MeV}}{pc}\right)^2 \frac{\rho c}{X_0} \cdot I. \tag{68}$$

Here, ρ is the mass density and X_0 the radiation length of the residual gas in units of g/m^2; c denotes the velocity of light, p the particle momentum, and $< \beta >$ the average beta function around the ring. The reader should be aware that this representation of gas scattering by a diffusion process in the I_x-I_z plane is a rough approximation,[4] though adequate for the present purpose.

In Fig. 8a the enhancement factor $\sin^2\chi/\sin^2\psi$, Eq. (29), is depicted as a function of the expression on the left hand side of Eq. (25). Condition (25) is fulfilled for two resonances only (out of 28), for which the external diffusion is enhanced by a modest factor of about 2–4.

If the residual gas is hydrogen, and for a pressure of $p_{H_2} \approx 10^{-9}$ mbar, one finds

$$D_{\rm ext}(I) \approx 2.5 \cdot 10^{-7} I \text{ mm mrad s}^{-1}. \tag{69}$$

Fig. 8b shows the diffusion coefficient along the chaotic layer $D_{\rm along}(I)$, Eq. (29), for all the resonances under consideration. It should be mentioned that only one of the resonances determined for HERA belongs to the plateau regime defined by

inequalities (31) and (32). The diffusion enhancement for this resonance is about a factor of 2.

3.9 Arnold Diffusion

The local diffusion coefficient $D_{\mathrm{Arnold}}(I)$ due to Arnold diffusion, Eq. (112), is depicted in Fig. 9 for $|Q_{x0} - Q_{z0} - m| \approx 0.005$ and for a linear coupling strength $\kappa = 0.005$. Note that this diffusion takes place in the stochastic layer around each resonance which covers only a small fraction of the phase space (see Fig. 3).

3.10 Comparison of Different Processes

The measured dynamic aperture of the HERA proton ring agrees remarkably well with the smallest value of action both at which modulational layers of overlapping sideband resonances are caused by synchrotron oscillations, for nonzero chromaticity, and at which stochastic layers of non-negligible width are generated around the primary resonances, due to power supply ripple.

Fig. 10 shows the diffusion coefficients calculated for modulational diffusion, resonance streaming, Arnold diffusion, and sweeping diffusion along with that for gas scattering. From the figure, it seems very unlikely that Arnold diffusion, resonance streaming, or sweeping diffusion is the source of the measured dynamic aperture since the corresponding diffusion rates are too small by many orders of magnitude. Only the diffusion coefficient for modulational diffusion is the right size to account for the observations. The range of values indicated for this coefficient reflects its strong dependence on the working point, in particular on the distance to the main coupling resonance. If modulational diffusion is the main source of the observed dynamic aperture, the beam lifetime at injection energy should depend not only on the working point, but also on the strength κ of the linear coupling resonance, on the chromaticity ξ, and on the momentum spread of the bunches. A strong sensitivity to all these parameters has in fact been observed.[21]

4 SUMMARY AND OUTLOOK

A semi-analytical approach has been described for the calculation of macroscopic transverse diffusion rates in proton storage rings, based on parameters of high-order resonances. Specific expressions of macroscopic diffusion coefficients have been derived assuming different local transport mechanisms such as modulational diffusion, resonance streaming, Arnold diffusion, and sweeping diffusion.

The evaluation of diffusion coefficients for the HERA proton ring shows that modulational diffusion due to synchrotron oscillations and nonzero chromaticity is the most probable explanation of the dynamic aperture measured.

ACKNOWLEDGEMENTS

I thank the members of the Accelerator Theory and Special Projects Department and of the Accelerator Department at SLAC for the friendly and exciting atmosphere. I am grateful to F. Willeke for stimulating discussions, and to F. Schmidt for various helpful comments and for a critical reading of the manuscript. É. Forest and M. Berz deserve my thanks for providing the Lie-algebra and differential-algebra program packages, respectively. Furthermore, I am indebted to W. Fischer and K. Heinemann for some useful remarks, to Y. Yan for his help in calculating the average Taylor map coefficients, to the DESY magnet group for making available the multipole data of the HERA magnets, and to the unknown referees whose comments helped to greatly improve the clarity and readability of this paper.

REFERENCES

1. M. Seidel, *Determination of Diffusion Rates in the Proton Beam Halo of HERA*, DESY HERA 93–04 (1993).
2. T. Chen et al., *Measurements of a Hamiltonian System and Their Description by a Diffusive Model*, Phys. Rev. Lett. **68** (1992) 33.
3. A. Gerasimov, *Diffusion Phenomenology of Transverse Beam Dynamics and Losses in Hadronic Colliders*, unpublished note (1991).

4. F. Zimmermann, *Emittance Growth and Proton Beam Lifetime in HERA*, DESY 93–59 (1993).

5. W. Fischer, M. Giovannozzi, and F. Schmidt, *Detailed Comparison of Experimental Observations and Computer Tracking for the SPS Dynamic Aperture Experiment*, to appear in the Proc. of the 1994 European Particle Accelerator Conference, London (1994).

6. A. Gerasimov,*The Applicability of Diffusion Phenomenology to Particle Losses in Hadron Colliders*, CERN SL/92–30 (1992).

7. B. V. Chirikov, *A Universal Instability of Many-Dimensional Oscillator Systems*, Physics Reports **52**, No. 5 (1979).

8. A. J. Lichtenberg and M. A. Lieberman, *Regular and Stochastic Motion*, Springer Verlag (1983).

9. B. V. Chirikov, M. A. Lieberman, D. L. Shepelyansky, and F. M. Vivaldi, *A Theory of Tune Modulation*, Physica **14D** (1985) 289–304.

10. J. Tennyson, *Resonance Transport in Near-Integrable Systems with Many Degrees of Freedom*, Physica **5D** (1982) 123–135.

11. A. Gerasimov, *Diffusive Transport Enhancement by Isolated Resonances and Distribution Tail Growth in Hadronic Beams*, Proc. of the 1991 IEEE Particle Accelerator Conference, San Francisco, and FERMILAB–Conf–90/250 (1991).

12. L. R. Evans and J. Gareyte, *The Beam-Beam Effect in the SPS*, CERN SPS 82–8 (DI-MST) (1982).

13. L. R. Evans, *The Beam-Beam Interaction*, CERN Accelerator School *Antiprotons in Colliding Beam Facilities*, Geneva 1984, CERN 84–15 (1984).

14. T. Chen and S. Peggs, *Beam-Beam Tune Modulation, the Driven Gravity Pendulum, and Josephson Junctions*, Proceedings of the third ICFA beam dynamics workshop, Novosibirsk (1989).

15. G. Ripken, F. Willeke, *Methods of Beam Optics*, DESY 88–114 (1988).

16. A. Schoch, *Theory of Linear and Nonlinear Perturbations of Betatron Oscillations in Alternating Gradient Synchrotrons*, CERN 57–21 (PS Division) (1958) 55–56.

17. M. Berz, *Differential-Algebraic Description of Beam Dynamics to Very High Orders*, Part. Acc. **24** (1989) 109;
Y. Yan and C. Yan, *ZLIB—A Numerical Library for Differential Algebra*, SSCL Report–300 (1990).

18. H. Brück et. al., Proc. EPAC 90, Nice (1990) 329.

19. J. Roßbach, *Fast Ground Motion at HERA*, DESY 89–023 (1989);
K. Flöttmann, Diploma Thesis, University of Hamburg, in German, DESY HERA 90–09

(1990);

W. Decking, Diploma Thesis, University of Hamburg, in German, DESY HERA 90–13 (1990).

20. R. Kleiss, F. Schmidt, and F. Zimmermann, *The Use of Truncated Taylor Maps in Dynamic Aperture Studies*, Part. Acc. **41** (1993) 117.
21. F. Willeke, private communication (1994).
22. R. D. Ruth, *Single-Particle Dynamics in Circular Accelerators*, AIP Conf. Proc. **153** (1987).
23. V. I. Arnold, Dokl. Akad. Nauk SSSR **144** (1962) 747; **148** (1963) 1257.
24. V. K. Melnikov, Dokl. Akad. Nauk SSSR **156** (1964) 9.
25. A. Wrulich, DESY 84–026 (1984).
26. F. Schmidt, CERN SL/90–52 (AP) (1991).
27. F. Schmidt, F. Zimmermann, and F. Willeke, *Comparison of Methods to Determine Long-Term Stability in Proton Storage Rings*, Part. Acc. **35** (1991) 249.
28. M. Hénon and C. Heiles, Astron. J. 69; 73 (1964), V.I. Oseledec, Trans. Moscow Math. Soc. 19 (1968) 197; G. Benettin et. al., Meccanica 15 (1980) 9, 21.
29. K. Wittenburg, *Experience with the Residual Gas Ionization Beam Profile Monitors at the DESY Proton Accelerators*, EPAC 92, Berlin, Vol. 2 (1994) 1133–1135.
30. F. Willeke, private communication (1991).
31. L. Burnod, G. Ferioli, J.B. Jeanneret, *Drift Speed Measurements of the HALO in the SPS Collider*, CERN/SL 90–01 (1990).
32. É. Forest, M. Berz, and J. Irwin, *Normal Form Methods for Complicated Periodic Systems: a Complete Solution using Differential Algebra and Lie Operators*, Part. Acc. **24** (1989) 91.
33. A. J. Dragt and J. M. Finn, *Lie Series and Invariant Functions for Analytic Symplectic Maps*, J. Math. Phys. **17** (1976) 2215–2227.

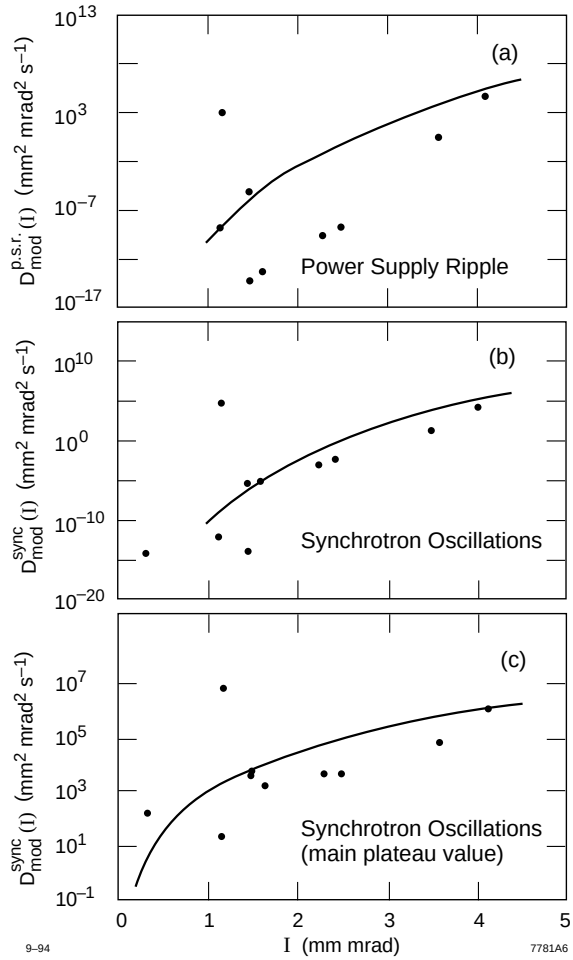

FIGURE 6: Diffusion coefficient $D_{\rm mod}(I)$ due to modulational diffusion as a function of the resonant action: a) assuming three overlapping sidebands at each fundamental resonance, a linear coupling $\kappa = 0.005$, a separation of tunes $|Q_{x0} - Q_{z0} - m| = 0.005$ and modulation parameters $q \approx 5 \cdot 10^{-5}$, $Q_m \approx 10^{-3}$, characteristic for power supply ripple; the curve represents the parametrization $D^{\rm p.s.r.}_{\rm mod}(I) \approx 5 \cdot 10^{-11} I^{25}$ (mm mrad)$^{-23}$ s^{-1}, b) assuming a linear coupling $\kappa = 0.005$, a separation of tunes $|Q_{x0} - Q_{z0} - m| = 0.005$ and modulation parameters $q \approx 2 \cdot 10^{-4}$, $Q_m \approx 4 \cdot 10^{-4}$ as due to synchrotron oscillations; represented are values for those resonances (17 out of 28) in APPENDIX D, for which both the first-order sidebands are large and the overlap condition is fulfilled (dots); the curve is the parametrization $D^{\rm sync}_{\rm mod}(I) \approx 5 \cdot 10^{-11} I^{25}$ (mm mrad)$^{-23}$ s^{-1}, which is the same parametrization as in the case of power supply ripple (Fig. b)), c) for a working point on the coupling resonance $|Q_{x0} - Q_{z0} - m| \approx 0$; the linear coupling $\kappa = 0.005$, and the modulation parameters $q \approx 2 \cdot 10^{-4}$ and $Q_m \approx 4 \cdot 10^{-4}$ are the same as in Fig. b); the curve represents the parametrization $D^{\rm sync}_{\rm mod}(I) \approx 10^3 I^5$ (mm mrad)$^{-3}$ s^{-1}. Note the large values of $D_{\rm mod}(I)$ for the single resonance at $I \approx 1.2$ mm mrad which are not covered by these parametrizations.

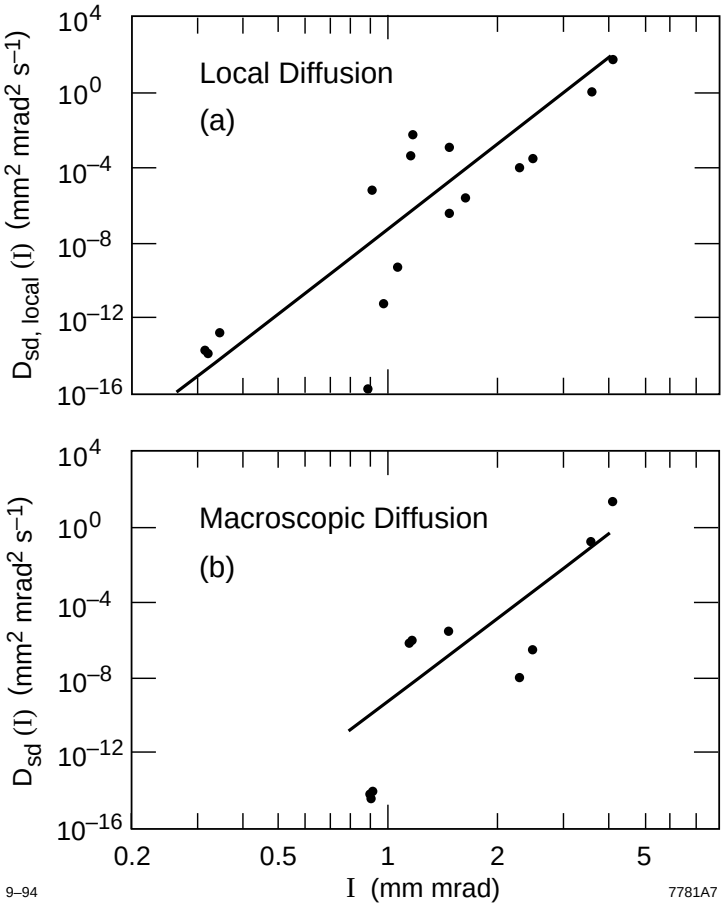

FIGURE 7: Sweeping diffusion: a) local diffusion coefficient $D_{\mathrm{sd,\ local}}(I)$, Eq. (21), inside the chaotic layer as a function of the resonant action; a modulation amplitude $q = 5 \cdot 10^{-5}$ is assumed; the curve represents the parametrization $D_{\mathrm{sd,local}}(I) \approx 5 \cdot 10^{-8} I^{15}$ (mm mrad)$^{-13}$ s^{-1}, b) macroscopic diffusion coefficient $D_{\mathrm{sd}}(I)$ as a function of the action in units of mm mrad for the resonances listed in APPENDIX D (dots); a modulation frequency $Q_m = 10^{-3}$ as that due to power supply ripple is assumed; the diffusion coefficient $D_{\mathrm{sd}}(I)$ is parametrized by the function $D_{\mathrm{sd}}(I) \approx 4 \cdot 10^{-10} I^{15}$ (mm mrad)$^{-13}$s^{-1} (line). The averaging of the local coefficient is strictly valid only for $I \leq 2$ mm mrad, while at even smaller amplitudes, below $I_0 \approx 0.7$ mm mrad, the phase space is entirely covered by regular trajectories and there is no sweeping diffusion.

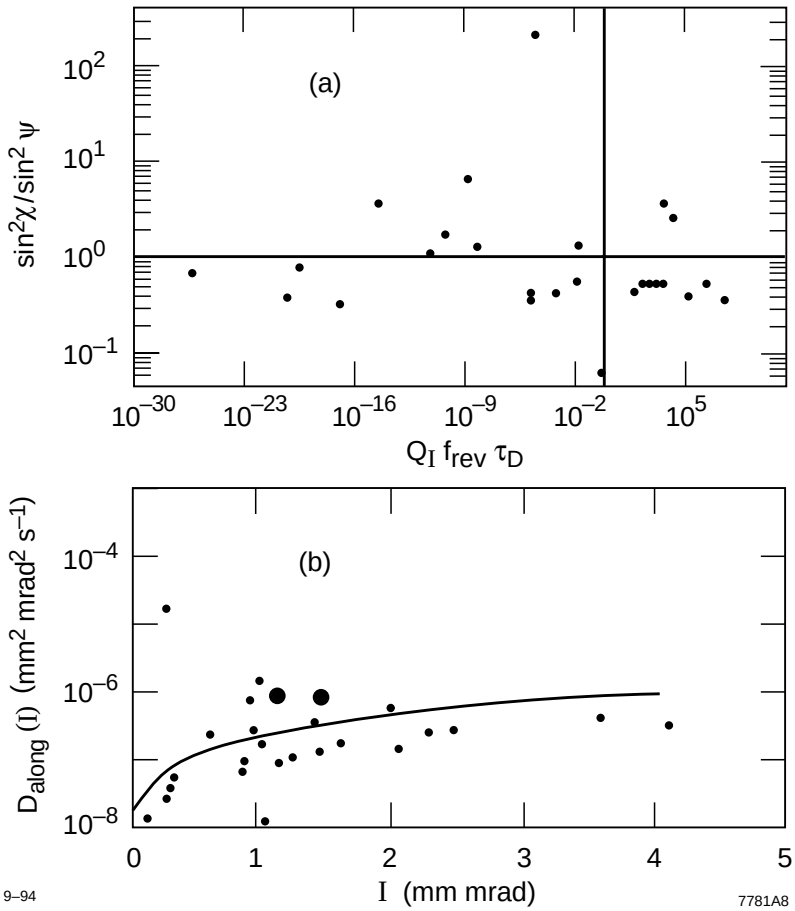

FIGURE 8: Resonance Streaming: a) diffusion enhancement factor $\sin^2\chi/\sin^2\psi$ versus the term $Q_I f_{rev}\tau_D$; only for the two resonances in the upper right corner enhanced diffusion due to resonance streaming is expected, b) diffusion coefficient $D_{\rm along}(I)$, Eq. (29), as a function of action for the resonances listed in APPENDIX D (dots); the curve represents the external diffusion caused by residual gas scattering, Eq. (68); the two large full circles indicate those resonances for which the external diffusion is enhanced; the small dots represent resonances without enhancement.

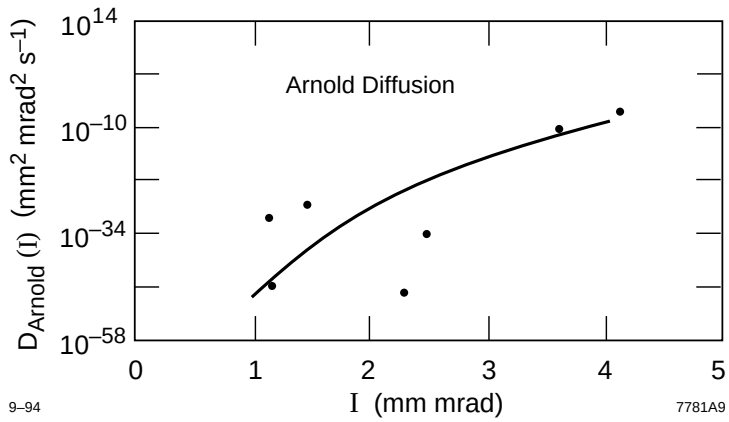

FIGURE 9: Diffusion coefficient $D_{\mathrm{Arnold}}(I)$ for Arnold diffusion driven by the main coupling resonance as a function of the action for the resonances listed in APPENDIX D (dots). The curve represents the parametrization $D_{\mathrm{Arnold}}(I) \approx 3 \cdot 10^{-49} I^{65}$ (mm mrad)^{2}s^{-1}.

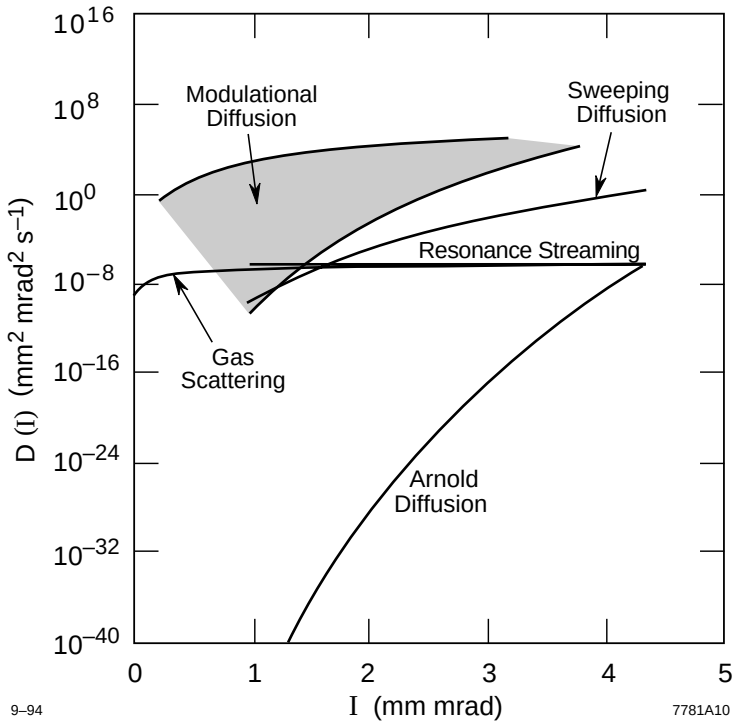

FIGURE 10: Comparison of diffusion coefficients computed for different types of nonlinear transport mechanisms and for gas scattering ($p_{H_2} = 10^{-9}$ mbar) as a function of action. While the coefficients for modulational and for sweeping diffusion are calculated as an average of the local diffusion coefficients over regular and chaotic phase space regions, those shown for resonance streaming and Arnold diffusion refer only to the region close to a resonance or inside the chaotic layer, respectively, and would be reduced (by about a factor 10–1000) if averaged over the phase space (compare also Fig. 3).

Under normal operating conditions, the transverse phase space for a large proton storage ring is covered by a web of weak, isolated resonance islands. Close to one of these resonances, $kQ_x + lQ_z \approx p$, the transverse motion can be described by the nonlinear Hamiltonian (see for instance Refs. [16,22])

$$\begin{aligned} H(I_x, I_z, \phi_x, \phi_z, \theta) &= I_x Q_{x0} + I_z Q_{z0} + g(I_x, I_z) + \\ &+ h(I_x, I_z)\cos(k\phi_x + l\phi_z - p\theta) + q \cdot (I_x + I_z) \cdot \cos(Q_m\theta + \alpha) \end{aligned} \tag{70}$$

where the last term represents an additional tune modulation of amplitude q and frequency Q_m in both transverse planes. The terms I_x and I_z designate the horizontal and vertical actions, respectively; ϕ_x and ϕ_z are the corresponding angle variables; and θ denotes the azimuthal position around the storage ring. The modulation frequency Q_m and amplitude q as well as the linear betatron tunes Q_{x0} and Q_{z0} are given in units of the revolution frequency. The nonlinear functions h and g, which depend only on the action variables, are called detuning and driving term, respectively. For typical high-order resonances, the detuning term g is much larger than the driving term h. The latter determines the maximum change rate of the action variables,

$$\left|\frac{dI_x}{d\theta}\right|_{\max} = \left|\frac{\partial H}{\partial \phi_x}\right|_{\max} = |k|\ h \quad , \quad \left|\frac{dI_z}{d\theta}\right|_{\max} = \left|\frac{\partial H}{\partial \phi_z}\right|_{\max} = |l|\ h, \tag{71}$$

and characterizes the strength of the resonance, while the detuning term g represents the amplitude-dependence of the horizontal and vertical tunes via

$$Q_x \approx \left\langle \frac{d\phi_x}{d\theta} \right\rangle_\theta = \left\langle \frac{\partial H}{\partial I_x} \right\rangle_\theta = Q_{x0} + \frac{\partial g}{\partial I_x}(I_x, I_z), \tag{72}$$

$$Q_z \approx \left\langle \frac{d\phi_z}{d\theta} \right\rangle_\theta = \left\langle \frac{\partial H}{\partial I_z} \right\rangle_\theta = Q_{z0} + \frac{\partial g}{\partial I_z}(I_x, I_z). \tag{73}$$

The resonance condition is exactly fulfilled at the resonant action values $I_{x,r}$ and $I_{z,r}$ which are given by

$$k\left(Q_{x0} + \frac{\partial g}{\partial I_x}(I_{x,r}, I_{z,r})\right) + l\left(Q_{z0} + \frac{\partial g}{\partial I_z}(I_{x,r}, I_{z,r})\right) = p. \tag{74}$$

Equation (74) defines the *resonance contour* in the I_x-I_z plane. For $k \neq 0$ the generating function

$$F(\bar{I}_x, \bar{I}_z, \phi_x, \phi_z, \theta) = (k\phi_x + l\phi_z - p\theta)\bar{I}_x + \phi_z \bar{I}_z \tag{75}$$

introduces new canonical variables $\bar{\phi}_x, \bar{\phi}_z, \bar{I}_x, \bar{I}_z$ according to

$$\bar{\phi}_x = \frac{\partial F}{\partial \bar{I}_x} = k\phi_x + l\phi_z - p\theta \quad , \quad \bar{\phi}_z = \frac{\partial F}{\partial \bar{I}_z} = \phi_z \tag{76}$$

$$I_x = \frac{\partial F}{\partial \phi_x} = k\bar{I}_x \quad , \quad I_z = \frac{\partial F}{\partial \phi_z} = l\bar{I}_x + \bar{I}_z \tag{77}$$

and a new Hamiltonian $\bar{H}$, which is independent of θ and reads

$$\begin{aligned} \bar{H}(\bar{I}_x, \bar{I}_z, \bar{\phi}_x, \bar{\phi}_z) &= (kQ_{x0} + lQ_{z0} - p)\bar{I}_x + \bar{I}_z Q_{z0} + \bar{g}(\bar{I}_x, \bar{I}_z) + \bar{h}(\bar{I}_x, \bar{I}_z)\cos(\bar{\phi}_x) \\ &+ q \cdot (k+l) \cdot \bar{I}_x \cdot \cos(Q_m\theta + \alpha) + q \cdot \bar{I}_z \cdot \cos(Q_m\theta + \alpha) \end{aligned} \tag{78}$$

where the barred functions $\bar{g}$ and $\bar{h}$ are related to the un-barred ones by

$$\bar{g}(\bar{I}_x, \bar{I}_z) \equiv g(k\bar{I}_x, l\bar{I}_x + \bar{I}_z) = g(I_x, I_z) \tag{79}$$

$$\bar{h}(\bar{I}_x, \bar{I}_z) \equiv h(k\bar{I}_x, l\bar{I}_x + \bar{I}_z) = h(I_x, I_z). \tag{80}$$

For $k = 0$ the function

$$F(\tilde{I}_x, \tilde{I}_z, \phi_x, \phi_z, \theta) = (k\phi_x + l\phi_z - p\theta)\tilde{I}_z + \phi_x \tilde{I}_x \tag{81}$$

generates a similar transformation. The new Hamiltonian (78) virtually describes a system of one degree of freedom, because the action $\bar{I}_z$ is an invariant of the motion. If we disregard the $\bar{I}_z$-$\bar{\phi}_z$ motion for the moment, in the absence of tune modulation ($q = 0$) and close to the resonance the motion in the $\bar{I}_x$-$\bar{\phi}_x$ plane can be approximated by a nonlinear pendulum,[7]

$$\bar{K}(\bar{\Delta}, \bar{\phi}) = \frac{1}{2}\frac{\partial^2 \bar{g}}{\partial \bar{I}_x^2}(\bar{I}_{x,r}, \bar{I}_{z,r})\bar{\Delta}_x^2 + \bar{h}(\bar{I}_{x,r}, \bar{I}_{z,r})\cos\bar{\phi}_x, \tag{82}$$

where we have defined the new momentum $\bar{\Delta}_x$ as the deviation of the action $\bar{I}_x$ from the resonant value,

$$\bar{\Delta}_x = \bar{I}_x - \bar{I}_{x,r}. \tag{83}$$

The pendulum motion (82) is characterized by two parameters, the half island width $\bar{\Delta}_{x,\max}$ and the island tune Q_I. The former is given by

$$\bar{\Delta}_{x,\max} = 2\left(\frac{h}{|\partial^2\bar{g}/\partial\bar{I}_x^2|}\right)^{\frac{1}{2}} = 2\left(\frac{h}{|l^2\frac{\partial^2 g}{\partial I_z^2} + 2kl\frac{\partial^2 g}{\partial I_x \partial I_z} + k^2\frac{\partial^2 g}{\partial I_x^2}|}\right)^{\frac{1}{2}} \tag{84}$$

and translates into a total island width in the original I_x-I_z plane via

$$\Delta I_{\text{tot}} \equiv 2\bar{\Delta}_{x,\max}\sqrt{k^2+l^2} = 4\left(\frac{(l^2+k^2)h}{|l^2\frac{\partial^2 g}{\partial I_z^2} + 2kl\frac{\partial^2 g}{\partial I_x \partial I_z} + k^2\frac{\partial^2 g}{\partial I_x^2}|}\right)^{\frac{1}{2}}. \tag{85}$$

The second parameter — the island tune Q_I — designates the frequency at which particles inside a resonance island oscillate around the elliptic fixed point.[14] It is given by

$$Q_I = \left[k^2\frac{\partial^2 g}{\partial I_x^2} + 2kl\frac{\partial^2 g}{\partial I_x \partial I_z} + l^2\frac{\partial^2 g}{\partial I_z^2}\right]^{\frac{1}{2}} h^{\frac{1}{2}}, \tag{86}$$

where the second order partial derivatives of g and the driving term h are evaluated at the resonance.

APPENDIX B LOCAL DIFFUSION COEFFICIENTS

APPENDIX B.1 Modulational Diffusion

The local coefficient $D_{\text{mod. local}}(I)$ for modulational diffusion can be calculated following Chirikov[8] and Lichtenberg.[9] As a starting point, for $k \neq 0$ we choose the Hamiltonian

$$\begin{aligned} H(\bar{\Delta}_x, \bar{\phi}_x, \bar{I}_z, \bar{\phi}_z, \theta) &= \frac{1}{2}\frac{\partial^2 g}{\partial \bar{I}_x^2}\bar{\Delta}_x^2 + h\cos\bar{\phi}_x + q\bar{\Delta}_x(k+l)\cos Q_m\theta \\ &+\kappa I_{x,r}^{\frac{1}{2}} I_{z,0}^{\frac{1}{2}} \cos\left(\frac{1}{k}\bar{\phi}_x - \frac{l}{k}\bar{\phi}_z + \frac{p}{k}\theta - m\theta - \bar{\phi}_z + \chi_0\right) + \bar{I}_z Q_{z0} \end{aligned} \tag{87}$$

where $\bar{\Delta}_x \equiv \bar{I}_x - \bar{I}_{x,r}$ is the deviation from the resonant value and χ_0 an initial phase. The Hamiltonian (87) is obtained by approximating the $\bar{I}_x$-$\bar{\phi}_x$ motion in Eq. (78) by a nonlinear pendulum of the form (82) and supposing, in addition, that the driving term $h_{\text{coupl}}(I_x, I_z)$ of the main coupling resonance $Q_x - Q_z = m$, Eq. (15), gives rise to the pump diffusion along $\bar{I}_z$.

The stochastic modulational layer extends over all overlapping sideband resonances, which can lead to a significant diffusion rate. In order to calculate it, the Hamiltonian of Eq. (87) may be decomposed into two parts,

$$\begin{aligned} H_{\rm across}(\bar{\Delta}_x, \bar{\phi}_x, \theta) &= \frac{1}{2}\frac{\partial^2 g}{\partial \bar{I}_x^2}\bar{\Delta}_x^2 + h\cos\left(\bar{\phi}_x + \frac{q\ (k+l)}{Q_m}\sin Q_m\theta\right) \\ H_{\rm along}(\bar{I}_z, \bar{\phi}_z, \theta) &= \bar{I}_z Q_{z0} + \kappa I_{x,r}^{\frac{1}{2}} I_{z,0}^{\frac{1}{2}}\cos\left(\frac{1}{k}\bar{\phi}_x(\theta) - \frac{l}{k}\bar{\phi}_z + \frac{p}{k}\theta - \right. \\ & \left. -m\theta - \bar{\phi}_z + \chi_0\right) \end{aligned} \tag{88}$$

where the change of $\bar{\phi}_x$ due to $H_{\rm across}$ drives the motion along the stochastic layer via $H_{\rm along}$. Canonical perturbation theory can be used to derive $\bar{\phi}_x$.[8] In zeroth order we find

$$H_{\rm across,0} = \frac{1}{2}\frac{\partial^2 g}{\partial \bar{I}_x^2}\bar{\Delta}_x^2, \tag{89}$$

which gives

$$\begin{aligned} \bar{\Delta}_{x,0} &= \text{const.}, \\ \bar{\phi}_{x,0} &= (\partial^2 g/\partial \bar{I}_x^2)\ \bar{\Delta}_{x,0}\theta. \end{aligned} \tag{90}$$

To first order in h the angle $\bar{\phi}_x$ reads

$$\bar{\phi}_x = \frac{\partial^2 g}{\partial \bar{I}_x^2}\bar{\Delta}_{x,0}\theta + h\sum_n \frac{J_n\left(\frac{q(k+l)}{Q_m}\right)}{\left(nQ_m + \bar{\Delta}_{x,0}\frac{\partial^2 g}{\partial \bar{I}_x^2}\right)^2}\sin\left(\frac{\partial^2 g}{\partial \bar{I}_x^2}\bar{\Delta}_{x,0}\theta + nQ_m\theta\right). \tag{91}$$

The argument of the cosine in $H_{\rm along}$ may now be written

$$\begin{aligned} \phi(\theta) &\equiv \frac{1}{k}\bar{\phi}_x(\theta) - \frac{l}{k}\bar{\phi}_z - \bar{\phi}_z + \frac{p}{k}\theta - m\theta + \chi_0 \\ &\approx \frac{1}{k}\frac{\partial^2 g}{\partial \bar{I}_x^2}\bar{\Delta}_{x,0}\theta - (Q_{x0} - Q_{z0} - m)\theta + \chi_0 + \\ &\quad + \frac{h}{k}RJ_\lambda(\lambda)\frac{1}{\left(\lambda Q_m + \bar{\Delta}_{x,0}\frac{\partial^2 g}{\partial \bar{I}_x^2}\right)^2}\sin\left(\frac{\partial^2 g}{\partial \bar{I}_x^2}\bar{\Delta}_{x,0}\theta + \lambda Q_m\theta\right). \end{aligned} \tag{92}$$

Here, $\lambda \equiv |k+l|\ q/Q_m$, and we have replaced $J_n\left(\frac{q\ (k+l)}{Q_m}\right)$ of Eq. (91) by the typical value $J_\lambda(\lambda) \approx \frac{1}{2}\lambda^{-\frac{1}{3}}$. R denotes an 'effective' number of resonances (in the application to HERA we have assumed $R \approx (2\lambda+1)$, that is $R \approx 3$ in the case of power supply ripple and $R \approx 4$–12 for synchrotron oscillations). The change of

$H_{\rm along}$ during the time $T \equiv \Theta/(2\pi f_{rev})$ is about

$$\begin{aligned}
\Delta H_{\rm along} &= \int_{-\Theta}^{\Theta} \frac{\partial}{\partial\theta} H_{\rm along}\, d\theta \\
&= \kappa I_{x,r}^{\frac{1}{2}} I_{z,0}^{\frac{1}{2}} \left[\cos\phi(\Theta) - \cos\phi(-\Theta) - \left(1+\frac{l}{k}\right) Q_{z0} \int_{-\Theta}^{\Theta} \sin\phi\, d\theta \right] \\
&\approx -\kappa I_{x,r}^{\frac{1}{2}} I_{z,0}^{\frac{1}{2}} \left(1+\frac{l}{k}\right) Q_{z0} \int_{-\Theta}^{\Theta} \sin\phi\, d\theta \qquad (93)
\end{aligned}$$

and the integrand in (93) reads

$$\begin{aligned}
\sin\phi(\theta) &= \sum_j A_j(\bar{\Delta}_{x,0}) \sin\left[\left(\frac{1}{k} \frac{\partial^2 g}{\partial \bar{I}_x^2} \bar{\Delta}_{x,0} - (Q_{x0} - Q_{z0} - m) + \right.\right. \\
&\left.\left. + j \frac{\partial^2 g}{\partial \bar{I}_x^2} \bar{\Delta}_{x,0} + j\lambda Q_m \right) \theta + \chi_0 \right] \qquad (94)
\end{aligned}$$

where

$$A_j(\bar{\Delta}_{x,0}) \equiv J_j \left[\frac{h}{k} \frac{R}{\left(\lambda Q_m + \bar{\Delta}_{x,0} \frac{\partial^2 g}{\partial \bar{I}_x^2}\right)^2} \frac{1}{2} \lambda^{-\frac{1}{3}} \right]. \qquad (95)$$

The diffusion rate in I_z is now obtained by averaging over the width of the modulational layer $\Delta \bar{I}_{\rm mod} \equiv 2\bar{\Delta}_{x,0,\max} \approx 2\lambda Q_m / |\frac{\partial^2 \bar{g}}{\partial \bar{I}_x^2}|$:[9,8]

$$\begin{aligned}
D_z &= \lim_{\Theta\to\infty} \left\langle \frac{2\pi f_{rev} (\Delta H_{\rm along})^2}{2Q_{z0}^2 (2\Theta)} \right\rangle_{\bar{\Delta}_{x,0},\ \chi_0} \\
&= \lim_{\Theta\to\infty} \left\langle \frac{2\pi f_{rev}}{4\Theta} \frac{\kappa^2 I_{x,r} I_{z,0}}{2\frac{\lambda Q_m}{|\frac{\partial^2 \bar{g}}{\partial \bar{I}_x^2}|}} \int_{-\lambda Q_m/|\frac{\partial^2 \bar{g}}{\partial \bar{I}_x^2}|}^{\lambda Q_m/|\frac{\partial^2 \bar{g}}{\partial \bar{I}_x^2}|} d\bar{\Delta}_{x,0} \left(1+\frac{l}{k}\right)^2 \cdot \right. \\
&\left. \cdot \int_{-\Theta}^{+\Theta} d\theta'' \sin\phi(\theta'') \int_{-\Theta}^{+\Theta} d\theta' \sin\phi(\theta') \right\rangle_{\chi_0} \qquad (96)
\end{aligned}$$

where the integration over θ'' yields a delta function

$$\begin{aligned}
\int_{-\infty}^{\infty} d\theta'' \sin\phi(\theta'') &= \sum_j A_j(\bar{\Delta}_{x,0}) \sin\chi_0 \frac{2\pi}{\left|\frac{1}{k}+j\right| \frac{\partial^2 \bar{g}}{\partial \bar{I}_x^2}} \cdot \\
&\cdot \delta\left(\bar{\Delta}_x - \frac{(Q_{x0} - Q_{z0} - m) - j\lambda Q_m}{\left(\frac{1}{k}+j\right) \frac{\partial^2 \bar{g}}{\partial \bar{I}_x^2}} \right). \qquad (97)
\end{aligned}$$

The integration over $\bar{\Delta}_{x,0}$ in Eq. (96) is readily performed,

$$D_z = \frac{\pi^2 f_{rev}\kappa^2 I_{x,r} I_{z,0}\left(1+\frac{l}{k}\right)^2}{\lambda Q_m} < \sin^2\chi_0 >_{\chi_0} \cdot \cdot \sum_{j=\tilde{l}}^{\infty} \frac{1}{\left|\frac{1}{k}+j\right|} A_j^2 \left(\frac{Q_{x0}-Q_{z0}-m-j\lambda Q_m}{\left(\frac{1}{k}+j\right)\frac{\partial^2 g}{\partial I_x^2}}\right) \frac{1}{2\Theta}\int_{-\Theta}^{\Theta} d\theta', \tag{98}$$

where $j=\tilde{l}$, with

$$\tilde{l} = \text{integer part}\left\{\frac{1}{2}\left[-\frac{1}{k}+\frac{Q_{x0}-Q_{z0}-m}{\lambda Q_m}\right]\right\}, \tag{99}$$

is the dominant term in the sum over j, and after averaging over χ_0 we obtain the approximate result

$$D_z \approx \frac{\pi^2 f_{rev}}{2}\frac{\kappa^2 I_{x,r} I_{z,0}\left(1+\frac{l}{k}\right)^2}{\lambda Q_m\left|\frac{1}{k}+\tilde{l}\right|} J_{\tilde{l}}^2\left[\frac{h}{2k^3}\frac{R\lambda^{-\frac{1}{3}}(1+\tilde{l}k)^2}{(Q_{x0}-Q_{z0}-m+\frac{\lambda}{k}Q_m)^2}\right]. \tag{100}$$

The total transverse diffusion rate is given by

$$D_{\text{mod, local}} = \left(\frac{l}{k}\frac{\frac{\partial^2 g}{\partial I_z^2}+\frac{\partial^2 g}{\partial I_z \partial I_x}}{\frac{\partial^2 g}{\partial I_x^2}+\frac{\partial^2 g}{\partial I_x \partial I_z}}-1\right)^2 D_z. \tag{101}$$

For $k=0$, $l\neq 0$ the diffusion rate reads

$$D_{\text{mod, local}} = D_x \approx \frac{\pi^2 f_{rev}}{2}\frac{\kappa^2 I_{x,r} I_{z,0}}{\lambda Q_m\left|\frac{1}{l}+\tilde{l}\right|} J_{\tilde{l}}^2\left[\frac{h}{2l^3}\frac{R\lambda^{-\frac{1}{3}}(1+\tilde{l}l)^2}{(Q_{x0}-Q_{z0}-m+\frac{\lambda}{l}Q_m)^2}\right] \tag{102}$$

where

$$\tilde{l} = \text{integer part}\left\{\frac{1}{2}\left[-\frac{1}{l}+\frac{Q_{x0}-Q_{z0}-m}{\lambda Q_m}\right]\right\}. \tag{103}$$

If the working point is chosen close to the coupling resonance, $Q_{x0}-Q_{z0}-m\approx 0$, we have $\tilde{l}=0$ and the diffusion coefficient $D_{\text{mod, local}}$, given by Eqs. (100) and (101), simplifies to

$$D_{\text{mod, local}}^{\text{plateau}} = \left(\frac{l}{k}\frac{\frac{\partial^2 g}{\partial I_z^2}+\frac{\partial^2 g}{\partial I_z \partial I_x}}{\frac{\partial^2 g}{\partial I_x^2}+\frac{\partial^2 g}{\partial I_x \partial I_z}}-1\right)^2 \frac{\pi^2 f_{rev}}{2}\frac{\kappa^2 I_{x,r} I_{z,0}\left(1+\frac{l}{k}\right)^2}{\lambda Q_m\left|\frac{1}{k}\right|}. \tag{104}$$

This is the maximum diffusion rate, which is known as 'main plateau value'[9,8] (not to be confused with the 'plateau regime' of resonance streaming).

As in the treatment of modulational diffusion, we suppose that the main coupling resonance $Q_x - Q_z = m$ drives the diffusion along the stochastic layer (compare Eq. (15)). The diffusion rate is obtained from[7,8]

$$D_{\text{Arnold}} \approx \frac{< (\Delta(I_x + I_z))^2 >}{2T}. \tag{105}$$

Here it has been assumed that for chaotic particles the phase χ_0 in Eq. (15) is completely random after a half period of oscillation around the elliptic fixed point.[8] The mean half period T for trajectories in the stochastic layer can be computed as an integral along the separatrix trajectory[23,24,7,8]

$$T = \frac{1}{2\pi f_{rev} Q_I} \ln \left| \frac{32\ e}{w_{\text{sl}}} \right|. \tag{106}$$

For $k \neq 0$ the change in I_z during the time T is obtained from

$$\begin{aligned}
\Delta I_z &\approx -\kappa I_x^{\frac{1}{2}} I_z^{\frac{1}{2}} \int_{-\infty}^{\infty} \sin(\phi_x - \phi_z - m\theta + \chi_0)\ d\theta \\
&\approx -\kappa I_x^{\frac{1}{2}} I_z^{\frac{1}{2}} \int_{-\infty}^{\infty} \sin\left(\frac{1}{k}\bar{\phi}_x + (Q_{x0} - Q_{z0} - m)\theta + \chi_0\right)\ d\theta \\
&\approx -\kappa I_x^{\frac{1}{2}} I_z^{\frac{1}{2}} \sin\chi_0 \frac{1}{Q_I} \int_{-\infty}^{\infty} \cos\left(\frac{1}{k}\bar{\phi}_x + (Q_{x,0} - Q_{z,0} - m)\theta\right) d\theta \\
&= -\kappa I_x^{\frac{1}{2}} I_z^{\frac{1}{2}} \sin\chi_0 \frac{1}{Q_I} \mathcal{A}_{\frac{2}{k}} \left(-\frac{Q_{x0} - Q_{z0} - m}{Q_I}\right).
\end{aligned} \tag{107}$$

Here, $\mathcal{A}_m(\lambda)$ denotes a Melnikov-Arnold integral, which for fractional $|m| << |\lambda|$ may be approximated by[7]

$$A_m(\lambda) \approx \frac{4\pi(2|\lambda|)^{|m|-1}}{\Gamma(|m|)} e^{\frac{-\pi|\lambda|}{2}}. \tag{108}$$

Averaging the squared change of action $(\Delta I_z)^2$ over the phase χ_0 yields

$$< (\Delta I_z)^2 >= \kappa^2 I_{x,r} I_{z,r} \frac{1}{2Q_I^2} \mathcal{A}^2_{\frac{2}{k}} \left(-\frac{Q_{x0} - Q_{z0} - m}{Q_I}\right). \tag{109}$$

Similarly, for $k = 0$ and $l \neq 0$ the change in I_x is calculated,

$$\begin{aligned}
\Delta I_x &\approx -\kappa I_x^{\frac{1}{2}} I_z^{\frac{1}{2}} \int_{-\infty}^{\infty} \sin(\phi_x - \phi_z - m\theta + \chi_0)\ d\theta \\
&\approx -\kappa I_x^{\frac{1}{2}} I_z^{\frac{1}{2}} \int_{-\infty}^{\infty} \sin\left(-\frac{1}{l}\bar{\phi}_z + (Q_{x0} - Q_{z0} - m)\theta + \chi_0\right)\ d\theta
\end{aligned}$$

$$
\begin{aligned}
&\approx \quad -\kappa I_x^{\frac{1}{2}} I_z^{\frac{1}{2}} \sin\chi_0 \frac{1}{Q_I} \int_{-\infty}^{\infty} \cos\left(-\frac{1}{l}\bar{\phi}_z + (Q_{x,0} - Q_{z,0} - m)\theta\right) d\theta \\
&= \quad -\kappa I_x^{\frac{1}{2}} I_z^{\frac{1}{2}} \sin\chi_0 \frac{1}{Q_I} \mathcal{A}_{-\frac{2}{l}} \left(-\frac{Q_{x0} - Q_{z0} - m}{Q_I}\right). \qquad (110)
\end{aligned}
$$

The mean squared change of the horizontal action is then

$$
< (\Delta I_x)^2 >= \kappa^2 I_{x,r} I_{z,r} \frac{1}{2Q_I^2} \mathcal{A}_{-\frac{2}{l}}^2 \left(-\frac{Q_{x0} - Q_{z0} - m}{Q_I}\right) \qquad (111)
$$

and the mean squared change of the sum of vertical and horizontal action is calculated as in Eq. (101)

$$
\begin{aligned}
< (\Delta(I_x + I_z))^2 > \quad &\approx \quad \left(1 - \frac{k}{l} \frac{\frac{\partial^2 g}{\partial I_x^2} + \frac{\partial^2 g}{\partial I_x \partial I_z}}{\frac{\partial^2 g}{\partial I_z^2} + \frac{\partial^2 g}{\partial I_z \partial I_x}}\right)^2 < (\Delta I_x)^2 > \quad \text{if } l \neq 0 \\
&\approx \quad \left(\frac{l}{k} \frac{\frac{\partial^2 g}{\partial I_z^2} + \frac{\partial^2 g}{\partial I_z \partial I_x}}{\frac{\partial^2 g}{\partial I_x^2} + \frac{\partial^2 g}{\partial I_x \partial I_z}} - 1\right)^2 < (\Delta I_z)^2 > \quad \text{if } k \neq 0. (112)
\end{aligned}
$$

APPENDIX C DYNAMIC APERTURE OF THE HERA PROTON RING

APPENDIX C.1 Computer Simulation Studies

The normal and skew multipole components through 32-poles have been measured for each of the about 600 s.c. HERA magnets. In computer simulations, the individual multipole components up to 20-poles of all s.c. dipoles and quadrupoles are taken into account by five thin, higher-order lenses in each FODO half cell. The strengths of the 6-, 10- and 12-pole correctors, independently powered in each quadrant, are added to the individual multipole coefficients of a magnet. This model of HERA is a very good approximation to the real machine.

The minimum time needed to inject 210 bunches into the HERA proton ring is some 20 minutes, corresponding to $6 \cdot 10^7$ turns. A typical number of turns in the tracking studies is 10^4, which requires about 15 minutes CPU time on an IBM 9000-720, using the computer codes RACETRACK[25] and SIXTRACK.[26] A promising method for early detection of chaotic trajectories consists in determining the rate of divergence of two initially close-by trajectories in phase space,[27] which is char-

acterized by the Lyapunov exponent.[28] Chaotic particles are potentially unstable and may experience an amplitude growth on a longer time scale.[4]

APPENDIX C.2 Measurement of the Dynamic and the Physical Aperture

After the beam is either excitated with the injection kicker or poorly injected such that a significant fraction of the beam is lost within the first few turns, the remaining protons completely fill the available aperture. The beam lifetime is then small (below one hour) and further excitation does not increase the beam emittance, but only causes additional particle losses. Under such conditions the beam profile observed with a residual-gas ionization monitor[29] is a direct measure of the aperture in HERA, be it dynamic or physical. Denoting the total width of the horizontal (or vertical) profile by $2r$, the aperture is simply

$$I_{\mathrm{da}}^{\mathrm{measured}} = \frac{r^2}{2\beta_{\mathrm{moni}}} \approx 0.5 - 0.8 \text{ mm mrad} \tag{113}$$

where β_{moni} designates the value of the beta function at the position of the monitor. The uncertainty shown on the right-hand side of Eq. (113) refers to the variations observed over periods of days and weeks, and not to the accuracy of the measurement, which is of the order of 5%. Since the measurement is performed for fully coupled beams (i.e., on the linear difference resonance $Q_x - Q_z = -1$) the aperture determined from the horizontal and the vertical profile monitor is about the same.

The bad beam lifetime after excitation indicates that Eq. (113) describes a dynamic and not a physical aperture limit. In order to verify this hypothesis, the physical aperture, as given by obstacles, has been measured in a different way. The closed beam orbit is distorted by slowly changing the strength of one of two orthogonal dipole steering coils (i.e., whose betatron phases are 90° apart) until the beam center reaches the physical aperture and all particles are lost. This gives an upper and a lower limit for the kick angle of either of the two steering correctors. The correctors are always set to the center value between the two limits found, and the measurement is iterated. Denoting the half-range between the two limits by θ_1 and θ_2 for the two correctors, respectively, a lower bound on the physical aperture

is given by

$$I_{\text{phys.},y} \geq \frac{1}{8\sin^2 \pi Q_y} \frac{\beta_{y,1}\theta_{y,1}^2 \beta_{y,2}\theta_{y,2}^2}{\beta_{y,1}\theta_{y,1}^2 + \beta_{y,2}\theta_{y,2}^2} \qquad (y = x, z), \tag{114}$$

where $\beta_{y,1}$ and $\beta_{y,2}$ denote the value of the beta function at the two correctors.[30] Inequality (114) follows from the closed orbit distortion induced by dipole kicks. The equal sign in Eq. (114) applies if the limit for both correctors is due to the same obstacle. In 1992 the physical aperture measured by this procedure was

$$I_{\text{phys.},x} \geq 1.50 \text{ mm mrad} \tag{115}$$

$$I_{\text{phys.},z} \geq 1.15 \text{ mm mrad.} \tag{116}$$

Comparison of Eqs. (116) and (113) shows that the dynamic aperture is considerably smaller than the physical aperture. Furthermore, the dynamic aperture is not very large when compared with the beam size, which corresponds to $I_{beam} \approx 0.25$ mm mrad (two standard deviations), but it turned out to be sufficient for stable beam operation.

APPENDIX C.3 Direct Evidence for Diffusion

The HERA collimator system can be used to directly measure the transverse diffusion rates as a function of amplitude.[1] For this purpose the collimators are moved towards the beam until they cut into the beam halo, and are then retracted by a few hundred microns. This method was previously used at the CERN SPS.[31]

In HERA, both after moving a collimator jaw into the beam and after retracting it, the observed background evolution at a scintillation counter is well parametrized by a diffusion equation of the form of Eq. (1).[1] A diffusion equation was also applied successfully to parametrize the beam profile evolution in the Fermilab Tevatron.[2]

APPENDIX C.4 Comparison of Measured and Simulated Dynamic Aperture

The predicted and the measured dynamic aperture of the HERA proton ring are shown in Fig. 11, as a function of the amplitude of momentum oscillation $\Delta p/p$. The upper dotted line represents the border above which particles are lost within $2 \cdot 10^4$

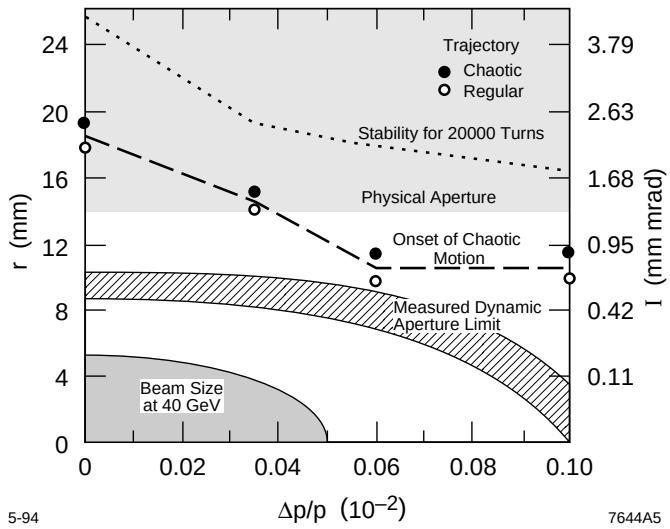

FIGURE 11: Dynamic aperture in the HERA proton ring: the dynamic aperture r expected from simulation studies, $r \equiv (2\beta(I_x + I_z))^{\frac{1}{2}}$ with $\beta = 76$ m, the two-sigma beam size and the actual dynamic aperture, as a function of the amplitude of momentum oscillations $\Delta p/p$. The range depicted for the measured aperture refers to the variation observed over periods of days or weeks.

turns in the simulation. About a factor of 2 smaller (for $\Delta p/p \approx 0$) is the amplitude at which the onset of chaotic particle motion is detected by the Lyapunov exponent method using 10^4 turns. This value was considered a conservative estimate of the dynamic aperture:

$$I_{\rm da}^{\rm simul} \approx 2.1 \ \ \text{mm mrad}. \tag{117}$$

To clearly distinguish the dynamic particle losses from those due to physical obstacles the tracking studies have been performed without introducing a physical aperture. In the amplitude region of the actual physical aperture the calculated particle trajectories are almost pure ellipses in the linearly decoupled phase space, the excursions of the linear invariants of motion (the nonlinear 'smear') being smaller than 1%.

While measurement and prediction of the dynamic aperture agree within a factor of 2, their difference is too large to be explained by uncertainties in the field errors, beam orbits, and the like. Rather, the difference indicates that some physical effect

has been omitted in the simulation. Tune modulation and slow drifts of parameters are two effects that have not been considered in the tracking studies which led to the estimate of Eq. (117).

When, in addition to the nonlinear field errors, a realistic tune modulation (of amplitude $q \approx 10^{-4}$ at a frequency of 50 Hz as that due to magnet current ripple) is also included in the simulation model, the dynamic aperture for on-momentum particles is considerably reduced,[4] and chaotic trajectories are found close to the actual dynamic aperture. In this case, the chaotic trajectories at amplitudes between 10 and 16 mm are interspersed among regular regions of phase space, so that tune modulation alone is not sufficient to cause a loss of all particles in this amplitude range. The latter can be explained by the additional slow drifts of the machine parameters which alter the positions of chaotic regions in phase space and thereby convert previously regular particles into chaotic ones and vice versa (compare Sections 2.4 and 3.4).

Neither the total impact of low-frequency tune modulation or synchrotron oscillations, nor the additional effect of parameter drifts can be reliably estimated by tracking studies for 10^4 turns. Here, an analytical treatment such as that described in this report may offer additional insight.

APPENDIX D NORMAL-FORM ANALYSIS AND PARAMETERS OF HIGH-ORDER RESONANCES IN HERA

Differential-algebra methods[17] in conjunction with normal-form algorithms[32] provide an efficient way to compute the Hamiltonian (70). Care has to be taken, however, since resonances of order lower than 11 may cause a divergence of the normal-form transformation. One possible approach[4] is to first perform an eighth order normalization and subsequently to rewrite the remainder as a Dragt-Finn factorization.[33] In other words, the original four-dimensional Taylor map M, extracted from the HERA model, is cast into the following form:

$$M = A^{-1} e^{:-2\pi QI + t_3(I) + \ldots + t_8(I):} e^{:f_9(I,\phi):} \ldots$$

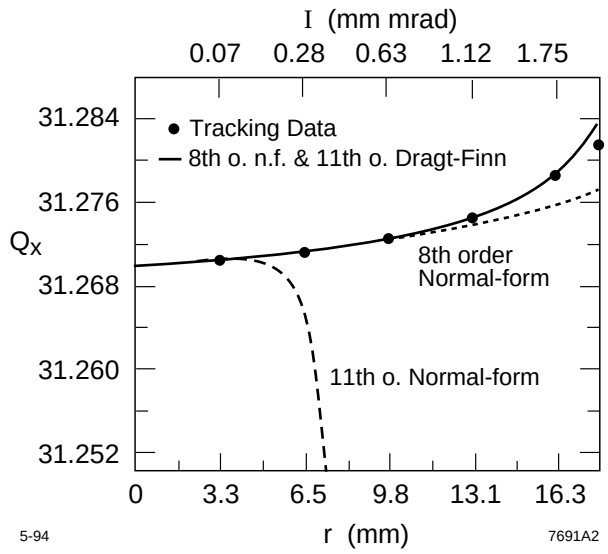

FIGURE 12: Horizontal tune Q_x obtained from tracking and from different normalization schemes as a function of amplitude $r \equiv (2\beta I_x)^{\frac{1}{2}}$, ($\beta = 76$ m, $I_z = 0$).

$$\ldots e^{:f_{11}(I,\phi):} A + \mathcal{O}(12), \tag{118}$$

where the t_n and f_n are polynomials of degree n in $y = \sqrt{2I_y}\cos\phi_y$, and $p_y = -\sqrt{2I_y}\sin\phi_y$ ($y = x, z$), and 'A' denotes the eighth order normal-form transformation. The tunes are given by the first partial derivatives with respect to $I_{x,z}$ of the approximate Hamiltonian

$$\begin{aligned} H_{\text{approx}} = A^{-1}[QI - \frac{1}{2\pi}\{t_3(I) + \ldots + t_8(I) + \\ + < f_9(I,\phi) + \ldots + f_{11}(I,\phi) >_\phi\}]. \end{aligned} \tag{119}$$

Here, the angular brackets indicate an average over $\phi_{x,z}$. Tune curves obtained by this method and those from an eighth and an eleventh order normal-form analysis are compared with the tracking data in Fig. 12. The divergence of the eleventh order normal-form analysis and the shortcoming of an eighth order normalization are evident, while the combination of a normal-form transformation and a Dragt-Finn factorization reproduces the amplitude-dependent tunes up to the threshold of chaotic motion found in the simulations without tune modulation.

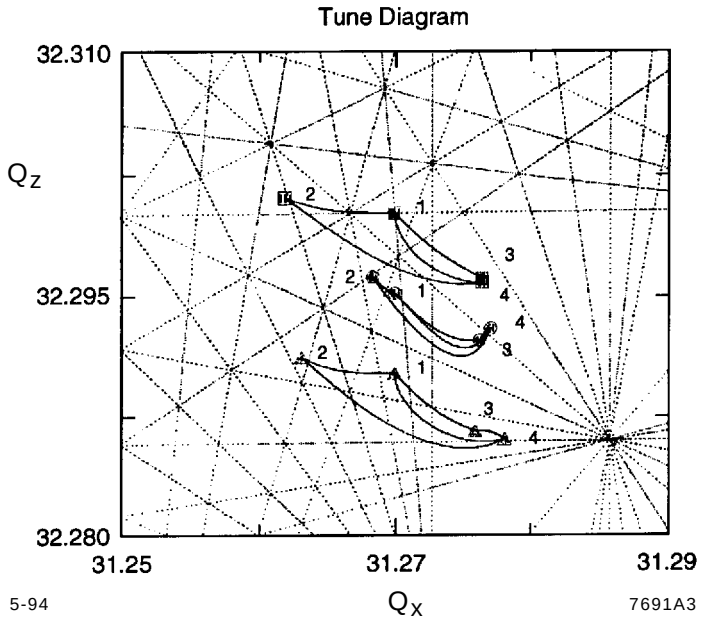

FIGURE 13: Diagram of the amplitude-dependent particle tunes for the HERA proton ring and of all resonance lines through order 11. The numbered dots indicate tunes for special values of the starting emittances, $(I_x, I_z) = 1)$ (0,0); 2) (0,2); 3) (2,0); 4) (2,2), in units of mm mrad. The connecting lines correspond to a continuous variation of the initial emittances between these values. The squares, circles and triangles refer to three different working points.

To identify the relevant high-order resonances the amplitude-dependent tunes are depicted for three different working points in Fig. 13. Also represented in the figure are all resonance lines through order 11. For the three working points, it is possible to identify 28 resonances of order 7 to 11, which are crossed by the tunes, if the starting action is changed continuously from 0 to 2 mm mrad along the three lines $I_x = 0$, $I_z = 0$, and $I_x = I_z$. In Section 3 we have used this set of resonances to determine typical values of certain quantities.

I_x	I_z	k	l	$\partial^2 g/\partial I_x^2$	$\partial^2 g/\partial I_x \partial I_z$	$\partial^2 g/\partial I_z^2$	h	Q_I
0.00	0.97	-3	6	$5 \cdot 10^{-3}$	$-4 \cdot 10^{-3}$	$2.6 \cdot 10^{-4}$	$2 \cdot 10^{-11}$	$2 \cdot 10^{-6}$
0.00	1.02	6	-2	$5 \cdot 10^{-3}$	$-4 \cdot 10^{-3}$	$2.9 \cdot 10^{-4}$	$1.3 \cdot 10^{-15}$	$2 \cdot 10^{-8}$
0.00	1.03	9	2	$5 \cdot 10^{-3}$	$-4 \cdot 10^{-3}$	$3 \cdot 10^{-4}$	$1.4 \cdot 10^{-24}$	$6 \cdot 10^{-13}$
0.00	1.06	3	4	$5.5 \cdot 10^{-3}$	$-4 \cdot 10^{-3}$	$3.2 \cdot 10^{-4}$	$1.3 \cdot 10^{-10}$	$2 \cdot 10^{-6}$
0.00	2.06	8	3	$8 \cdot 10^{-3}$	$-5.7 \cdot 10^{-3}$	$1.8 \cdot 10^{-2}$	$3.3 \cdot 10^{-21}$	$3 \cdot 10^{-11}$
0.32	0.00	7	-3	$3.3 \cdot 10^{-3}$	$-2.7 \cdot 10^{-3}$	$-7.1 \cdot 10^{-5}$	$9 \cdot 10^{-13}$	$5 \cdot 10^{-7}$
0.65	0.00	-4	7	$3.1 \cdot 10^{-3}$	$-2.2 \cdot 10^{-3}$	$-1.7 \cdot 10^{-4}$	$3 \cdot 10^{-17}$	$2 \cdot 10^{-9}$
0.90	0.00	11	0	$3 \cdot 10^{-3}$	$-2.0 \cdot 10^{-3}$	$-1.9 \cdot 10^{-4}$	$1.1 \cdot 10^{-8}$	$6 \cdot 10^{-5}$
0.57	0.57	7	-3	$3.9 \cdot 10^{-3}$	$-2.4 \cdot 10^{-3}$	$-2.7 \cdot 10^{-4}$	$1.6 \cdot 10^{-7}$	$2 \cdot 10^{-4}$
0.74	0.74	-4	7	$3.9 \cdot 10^{-3}$	$-2.1 \cdot 10^{-3}$	$-3.6 \cdot 10^{-4}$	$3.1 \cdot 10^{-7}$	$2 \cdot 10^{-4}$
1.24	1.24	11	0	$3.8 \cdot 10^{-3}$	$-1.3 \cdot 10^{-3}$	$-6.2 \cdot 10^{-4}$	$7.7 \cdot 10^{-8}$	$2 \cdot 10^{-4}$

TABLE 1: Parameters of high-order resonances in HERA as a function of action values I_x and I_z in units of mm mrad, for the working point $Q_x = 31.27$, $Q_z = 32.30$.

I_x	I_z	k	l	$\partial^2 g/\partial I_x^2$	$\partial^2 g/\partial I_x \partial I_z$	$\partial^2 g/\partial I_z^2$	h	Q_I
0.00	1.43	7	-3	$4 \cdot 10^{-3}$	$-1.2 \cdot 10^{-3}$	$7 \cdot 10^{-4}$	$1 \cdot 10^{-17}$	$2 \cdot 10^{-9}$
0.17	0.00	10	1	$3.4 \cdot 10^{-3}$	$-1.8 \cdot 10^{-6}$	$-7 \cdot 10^{-6}$	$2.8 \cdot 10^{-14}$	$1 \cdot 10^{-7}$
0.90	0.00	11	0	$2.9 \cdot 10^{-3}$	$-7.8 \cdot 10^{-5}$	$-2.3 \cdot 10^{-3}$	$1.1 \cdot 10^{-8}$	$6 \cdot 10^{-5}$
0.16	0.16	10	1	$3.4 \cdot 10^{-3}$	$-8.9 \cdot 10^{-5}$	$-2.1 \cdot 10^{-5}$	$6 \cdot 10^{-13}$	$5 \cdot 10^{-7}$
0.81	0.81	11	0	$2.9 \cdot 10^{-3}$	$-1.4 \cdot 10^{-4}$	$-4.5 \cdot 10^{-4}$	$7.2 \cdot 10^{-9}$	$5 \cdot 10^{-5}$
2.05	2.05	3	4	$1.6 \cdot 10^{-3}$	$6.8 \cdot 10^{-4}$	$-1.4 \cdot 10^{-3}$	$3.9 \cdot 10^{-5}$	$6 \cdot 10^{-4}$

TABLE 2: Parameters of high-order resonances in HERA as a function of action values I_x and I_z in units of mm mrad, for the working point $Q_x = 31.27$, $Q_z = 32.295$.

I_x	I_z	k	l	$\partial^2 g/\partial I_x^2$	$\partial^2 g/\partial I_x \partial I_z$	$\partial^2 g/\partial I_z^2$	h	Q_I
0.00	0.38	9	2	$4.1 \cdot 10^{-3}$	$-3.2 \cdot 10^{-3}$	$1 \cdot 10^{-4}$	$2.8 \cdot 10^{-29}$	$3 \cdot 10^{-15}$
0.00	0.95	7	-3	$5 \cdot 10^{-3}$	$-3.3 \cdot 10^{-3}$	$2.9 \cdot 10^{-4}$	$1.3 \cdot 10^{-19}$	$2 \cdot 10^{-10}$
0.00	1.26	8	3	$5.6 \cdot 10^{-3}$	$-3.5 \cdot 10^{-3}$	$5.4 \cdot 10^{-4}$	$2 \cdot 10^{-24}$	$6 \cdot 10^{-13}$
0.00	2.00	6	-2	$6.8 \cdot 10^{-3}$	$-4.3 \cdot 10^{-3}$	$1.7 \cdot 10^{-3}$	$2.5 \cdot 10^{-15}$	$3 \cdot 10^{-8}$
0.35	0.00	10	$+1$	$3.2 \cdot 10^{-3}$	$-2.6 \cdot 10^{-3}$	$-1.1 \cdot 10^{-4}$	$1.9 \cdot 10^{-12}$	$7 \cdot 10^{-7}$
0.88	0.00	1	6	$2.9 \cdot 10^{-3}$	$-1.8 \cdot 10^{-3}$	$-2.9 \cdot 10^{-4}$	$6.6 \cdot 10^{-14}$	$4 \cdot 10^{-8}$
0.91	0.00	11	0	$2.9 \cdot 10^{-3}$	$-2.8 \cdot 10^{-3}$	$-3 \cdot 10^{-4}$	$1.1 \cdot 10^{-8}$	$6 \cdot 10^{-5}$
0.58	0.58	1	6	$3.8 \cdot 10^{-3}$	$-2.2 \cdot 10^{-3}$	$-2.5 \cdot 10^{-4}$	$4.4 \cdot 10^{-7}$	$1 \cdot 10^{-4}$
0.74	0.74	10	1	$3.9 \cdot 10^{-3}$	$-1.9 \cdot 10^{-3}$	$-3.2 \cdot 10^{-4}$	$2.7 \cdot 10^{-9}$	$3 \cdot 10^{-5}$
1.14	1.14	11	0	$3.7 \cdot 10^{-3}$	$-1.3 \cdot 10^{-3}$	$-5.1 \cdot 10^{-4}$	$4.3 \cdot 10^{-8}$	$1 \cdot 10^{-4}$
1.79	1.79	0	7	$2.8 \cdot 10^{-3}$	$-4.7 \cdot 10^{-4}$	$-8.9 \cdot 10^{-4}$	$6.0 \cdot 10^{-6}$	$5 \cdot 10^{-4}$

TABLE 3: Parameters of high-order resonances in HERA as a function of action values I_x and I_z in units of mm mrad, for the working point $Q_x = 31.27$, $Q_z = 32.29$.